

Accurate calculation of dynamic Stark shifts and depopulation rates of Rydberg energy levels induced by blackbody radiation. Hydrogen, helium, and alkali-metal atoms

John W. Farley

Department of Physics and Optical Sciences Center, University of Arizona, Tucson, Arizona 85721

William H. Wing

*Joint Institute for Laboratory Astrophysics, Boulder, Colorado 80309
and Department of Physics and Optical Sciences Center, University of Arizona, Tucson, Arizona 85721*

(Received 6 June 1980)

A highly excited (Rydberg) atom bathed in blackbody radiation is perturbed in two ways. A dynamic Stark shift is induced by the off-resonant components of the blackbody radiation. Additionally, electric-dipole transitions to other atomic energy levels are induced by the resonant components of the blackbody radiation. This depopulation effect shortens the Rydberg-state lifetime, thereby broadening the energy level. Calculations of these two effects in many states of hydrogen, helium, and the alkali-metal atoms Li, Na, K, Rb, and Cs are presented for $T = 300$ K. Contributions from the entire blackbody spectrum and from both discrete and continuous perturbing states are included. The accuracy is considerably greater than that of previous estimates.

I. INTRODUCTION

A highly excited (Rydberg) atom bathed in a flux of blackbody radiation (BBR) is perturbed by the fluctuating electromagnetic field. The interaction between the atom and the BBR produces two principal effects. First, the off-resonant components of the BBR spectrum induce a dynamic Stark shift of the atomic energy levels. Second, the resonant components of the BBR spectrum drive electric-dipole transitions between atomic states. This depopulation effect shortens the effective atomic lifetimes, thereby broadening the homogeneous width of the energy levels.

The subtle effect of BBR on atoms is usually neglected in atomic physics. There are two plausible reasons for neglecting BBR effects. First, BBR has a very broad spectrum, whose width is approximately 10^{12} Hz at room temperature. Accordingly, BBR has very low spectral brightness and hence produces very feeble perturbations, compared to perturbations due to radiation from resonance lamps or from lasers. Second, there is a gross mismatch in frequency between ambient BBR and the atomic transitions most commonly studied: those involving the ground state. The former falls in the far infrared spectral region; the latter falls in the optical or ultraviolet region. The reduction in the effectiveness of any time-varying perturbation when the perturbation frequency is off resonance constitutes a second, superficially appealing argument for neglecting the effects of BBR.

On closer examination, however, BBR effects are not, in fact, always negligible. There are several reasons to expect enhanced effects in highly excited (Rydberg) atoms, whose properties

are different in many ways from those of ground-state atoms. Because Rydberg atoms have very large radii, electric-dipole transitions between Rydberg states have very large matrix elements. This increases the strength of the interaction between the atom and the BBR electric field. Also, transitions between Rydberg states often correspond to the microwave or infrared portion of the spectrum and are thus more closely matched to the BBR frequency spectrum than are transitions between low-lying states. Finally, even very small effects may become detectable by rapidly advancing ultrahigh-resolution spectroscopic techniques.

There is a small and yet incomplete body of recent theoretical and experimental work on BBR effects on atoms. We consider first the depopulation effects of BBR. Gallagher and Cooke¹ first pointed out that BBR may have non-negligible effects on Rydberg atoms, even at room temperature. They calculated the BBR-induced depopulation rates in the $17P$ and $18P$ states of sodium. This lifetime-shortening effect accounted for a factor-of-3 discrepancy between the experimental lifetimes of these states, as measured by Gallagher and Cooke, and the theoretical values calculated by Gounand.² In the latter calculation, BBR effects were neglected; the lifetime was calculated assuming radiative decay to be the sole decay mechanism.

Cooke and Gallagher³ derived a simple asymptotic formula to estimate the BBR-induced depopulation rate for very high Rydberg states. The formula gives a depopulation rate proportional to absolute temperature T and inversely proportional to the square of the principal quantum number n . In order to test the accuracy of the

formula, they performed a more accurate calculation of the BBR-induced depopulation rate for a few Rydberg states of sodium. They found that the asymptotic formula overestimates the rate, often quite badly. While the accuracy of the asymptotic formula improves slowly with increasing values of the principal quantum number n , accurate ($\sim 1\%$) values can only be obtained by direct calculation. To date, the literature contains only calculations by Cooke and Gallagher for a few isolated states. Much more valuable for connection with other work would be a systematic survey of BBR-induced depopulation rates over a wide range of quantum numbers and atomic species. The present paper constitutes such a study.

BBR-induced depopulation effects have been the subject of recent experiments. Beiting *et al.*,⁴ Gallagher and Cooke,⁵ and Cooke and Gallagher³ have observed BBR-induced redistribution of population among Rydberg levels. Gross *et al.*⁶ have observed amplification of BBR by small samples of high-Rydberg atoms. In these experiments, otherwise puzzling effects were attributed to room-temperature BBR.

More conclusive proof that the observed effects are, in fact, caused by BBR comes from experiments in which the ambient temperature is varied. Koch *et al.*⁷ passed an atomic beam containing long-lived Rydberg states through an oven and observed a temperature-dependent population distribution among the Rydberg states. Spencer⁸ made lifetime measurements of a single Rydberg state over a range of temperature and found a temperature-dependent lifetime. Related work has been done by Figger *et al.*⁹

The dynamic Stark shift induced by BBR has not yet been observed experimentally. The only theoretical calculation is an asymptotic estimate by Gallagher and Cooke,¹ who obtained an upward shift, common to all sufficiently high Rydberg levels in all atoms, of 2.2 kHz at a BBR temperature of 300 K. In this asymptotic estimate, the peculiarities of the atomic species do not appear, and the shift at low and intermediate values of n remains unknown. Until now, no accurate calculations of the dynamic Stark shift have been performed for any atomic state.

There exists a considerable body of related work in the field of optical pumping. Dynamic Stark shifts induced by the off-resonant spectral components of resonance lamps were first observed by Arditi and Carver.¹⁰ Dupont-Roc *et al.*¹¹ observed shifts of several tens of Hz, or more than twenty experimental linewidths. Kastler¹² wittily dubbed this effect the "lamp shift"; it is more commonly called the "light

shift." The detailed theory of light shifts in optical pumping experiments was worked out by Barrat and Cohen-Tannoudji¹³ and by Happer and coworkers.¹⁴

The theory of light shifts in optical pumping is, however, not directly applicable to the study of BBR-induced Stark shifts. Although both phenomena stem ultimately from the same quantum-mechanical interaction, the specialized approximations made in the optical pumping work render it inapplicable to the BBR case. Specifically, light shifts in optical pumping experiments are caused by a nearly resonant source. Consequently, the rotating-wave approximation is an appropriate simplification of the problem. In contrast, the appropriate approximations for studying BBR-induced Stark shifts are quite different. Because the bulk of the BBR spectrum is very far from resonance, the rotating and counter-rotating components of the radiation field make contributions of comparable magnitude. In the theory of BBR-induced dynamic Stark shifts, the rotating-wave approximation is therefore inappropriate, and we retain the antiresonant term in the equation for the shift.

In this paper we present accurate calculations of two effects induced by the BBR electric field: the dynamic Stark shift and the electric-dipole depopulation rate. The much smaller effects of the BBR *magnetic* field (dynamic Zeeman effect and magnetic dipole transitions) are neglected. We also neglect electric-quadrupole transitions, since they are slower than electric-dipole transitions, by a factor of order α^2 , for Rydberg as well as ground states. In Sec. II, we derive theoretical expressions accurate to lowest nonvanishing order in standard time-dependent perturbation theory. The BBR electric field is treated classically. Our treatment of the dynamic Stark shift does not make the usual rotating-wave approximation. The formalism is developed in full generality; it includes contributions from all components of the blackbody spectrum and from all perturbing states accessible via electric-dipole transitions, including those in the continuum. For convenience, we use the general term *perturbing states* to refer to intermediate states (in the calculation of the dynamic Stark shift) or final states (in the calculation of the depopulation rate). The sum over perturbing states consists of terms which factor into the square of the electric-dipole matrix element and a universal function, applicable to all atoms, which depends on atomic parameters solely through its argument. Approximate formulas are developed for both BBR effects, applicable in the high- n regime. The range of validity of our theoretical approach

is discussed. In Sec. III we present details of the evaluation of the electric-dipole matrix elements and the summation over discrete and continuous perturbing states. Section IV presents the results for many states of hydrogen, helium, and alkali-metal atoms. In Sec. V we compare our results with the results of others and discuss several cases of interest for high-precision spectroscopy. Appendix A contains details of the theory of the dynamic Stark shift, and Appendix B describes the evaluation by numerical integration of the universal function for the dynamic Stark shift.

II. THEORY

The interaction of an atom with the radiation field is a complex topic, and a host of complicated phenomena are known to occur at strong fields. In this paper, we shall deal only with weak fields. Our approach is valid to lowest nonvanishing order in perturbation theory. We sketch the outline of the development from first principles of the relevant equations. Much more detailed treatments can be found in standard references.¹⁵

The well-known starting point is a model system consisting of an isolated atom coupled to the quantized radiation field. The isolated atom is a wholly fictitious entity which would exist if one could somehow "turn off" the radiation field. The excited states of such an atom would not decay; their energies would be arbitrarily sharp. Each mode of the quantized radiation field has $n + \frac{1}{2}$ "photons", where the photon occupation number n represents blackbody photons present when $T > 0$ in thermal equilibrium, and $\frac{1}{2}$ represents the vacuum (zero-point) fluctuations that remain at $T = 0$.

The interaction of the vacuum fluctuations with the atom produces two well-known effects. First, the fluctuating electric field of the vacuum stimulates emission from excited atomic states.¹⁶ This spontaneous decay produces a finite lifetime of the excited states and, therefore, a nonzero level width. The second effect of the vacuum fluctuations is a radiative shift (Lamb shift) in the atomic energy levels. The effects of the vacuum fluctuations are taken into account by incorporating them into the atomic Hamiltonian. The decay of the excited states is included phenomenologically by adding a radiative damping term in the time-dependent Schrödinger equation. The radiative level shifts are included by adding small corrections to the values of the atomic energies. When these modifications are made to the atomic Hamiltonian, the vacuum fluctuations are then decoupled from the problem and

can be safely neglected thereafter.

We now detail our assumptions about the nature of the blackbody radiation field, which we treat classically. We assume the BBR is isotropic. Furthermore, we assume that any correlations between the phases of different spectral components of the radiation field average to zero. Consequently, the effect of the entire blackbody spectrum can be obtained by calculating the effect of a single frequency component, and integrating the result over the BBR frequency spectrum. A monochromatic off-diagonal perturbation is represented by $\hat{V} \cos \omega t$, where \hat{V} is given in the electric-dipole approximation by

$$\hat{V} = e\vec{r} \cdot \vec{E}/\hbar. \quad (1)$$

In Eq. (1), e is the absolute value of the electron charge and r is the radius vector of the electron. We shall neglect relaxation processes and treat energy levels as arbitrarily sharp. We calculate BBR effects on an atom at rest; i.e., we neglect the Doppler effect. This is justifiable because of the isotropy and very broad spectral distribution of the BBR, as long as the atomic speed is small compared to that of light.

A. The dynamic Stark effect

A time-varying electric field has effects on an atomic system which are qualitatively different from those of a static electric field. Because the Hamiltonian is explicitly time dependent, there are no eigenvalues. The time-dependent Schrödinger equation is a transient problem rather than an eigenvalue problem.

Since there are no eigenvalues, it makes little sense, strictly speaking, to refer to perturbation-induced shifts to eigenvalues. We will nevertheless speak of a shift in the energy of a state. This linguistic convention has the following meaning: An atom is imagined to be subjected to both a perturbing field and an arbitrarily weak probe field. In the absence of the perturbing field, the probe field would induce a Lorentzian resonance, whose line center is given by the energy difference between the relevant states. In the presence of the perturbing field, the probe field induces a resonance at a slightly different frequency. The frequency difference is referred to as the dynamic Stark shift. In addition, in the presence of the perturbing field, the probe field induces new resonances, which have no counterpart in the unperturbed case. Figuratively speaking, one can think of the perturbation as putting sidebands on the wave function. The new resonances represent multiple quantum transitions in which one photon is absorbed from the probe field and one or more from the perturbing field. For sufficient-

ly weak perturbations, these resonances are much less intense than the principal resonance. Consequently, they will be neglected in this work.

Our discussion of the dynamic Stark shift follows the approach of Townes and Schawlow.¹⁷ A similar approach was taken by Autler and Townes.¹⁸ We distinguish four different regimes depending on the relationship between the frequency of the perturbing field, the magnitude and width of atomic transitions, and the magnitude of the dynamic Stark shift. In the following discussion, references to "the" atomic interval implicitly refer to a two-level atom; realistic calculations require a sum over many levels.

Case I: Quasistatic perturbation. If the frequency of the perturbing electric field is much less than the natural linewidth of the atomic transition, the effect of the perturbation can be calculated at any instant as if it were static. The atomic system then follows the perturbing electric field adiabatically.

Case II: Slowly varying perturbation. If the frequency of the perturbing electric field is greater than the natural linewidth, but much less than the atomic interval, the system can no longer follow the variation of the electric field, but responds only to the average (rms) electric field. The probe field induces a shifted principal resonance and a number of weaker multiple-quantum resonances. The position of the principal resonance can be calculated as in Case I, using the average (rms) value of the electric field.

Case III: Rapidly varying nonresonant perturbation. When the frequency of the perturbation is much greater than both the linewidth and the quasistatic (Case I) Stark shift, and when the perturbation frequency ω is far from resonance, the shift $\delta\omega_a$ in the energy ω_a (in circular frequency units) of level a is given to lowest order in V by

$$\delta\omega_a(\omega) = \frac{1}{4} \sum_b |V_{ab}|^2 \left(\frac{1}{\omega_a - \omega_b - \omega} + \frac{1}{\omega_a - \omega_b + \omega} \right). \quad (2)$$

For a fuller discussion, see Eq. (36) of Ref. 18 or Eq. (10-77) of Ref. 17. Here $V_{ab} = \langle a | e\vec{r} \cdot \vec{E} | b \rangle / \hbar$. The symbols a and b represent the complete sets of quantum numbers of the atomic states a and b . We have not made the rotating-wave approximation; Equation (2) includes both the resonant and the antiresonant terms. The latter is responsible for the Bloch-Siegert shift¹⁹ in magnetic resonance experiments. The dynamic Stark shift depends on the frequency of the perturbation. The shift can be either positive or negative. The sign of the shift depends on whether the frequency of the perturbation is greater than or less than the frequency of the atomic transi-

tion. Equation (2) has poles at $\omega_a - \omega_b = \pm\omega$, which lie on the real axis as a result of neglecting radiative damping; we discuss this point further below.

Case IV: Resonant perturbation. When the perturbation is approximately resonant with an atomic transition, the problem can be solved for a two-level atom in the rotating-wave approximation. The wave function has two terms with different frequencies. Exactly on resonance, the two terms are of equal magnitude, and the two frequencies differ by the famous "Rabi flopping frequency." This is also variously termed the Autler-Townes effect or the production of Jaynes-Cummings doublets.²⁰ Away from resonance, the two terms are of very unequal magnitudes. The relative importance of the two terms reverses as the frequency of the perturbation sweeps through resonance. Neglecting the smaller of the two terms and radiative damping, we obtain a frequency-dependent dynamic Stark shift which executes a finite jump from one branch to the other at resonance.

For the purposes of calculating BBR-induced effects, the vast bulk of the spectrum of the perturbation varies rapidly enough that the relevant cases are Cases III and IV. Therefore we neglect the tiny regimes in which Cases I and II apply. The contribution to the dynamic Stark shift from the nonresonant parts of the BBR spectrum (Case III) is obtained by integrating Eq. (2) over the nonresonant parts of the BBR spectrum.

In order to calculate the contribution to the dynamic Stark shift from the near-resonant parts of the BBR spectrum, one can integrate the expression for Case IV over the near-resonant part of the spectral distribution. Assuming that the spectral distribution of the perturbation varies slowly over the resonance region, one finds that the contributions from the high-frequency and low-frequency side of the resonance largely cancel. The net contribution from a spectral region symmetric around the resonance is proportional to the frequency derivative of the spectral distribution; a flat perturbation spectrum gives no shift.

An equivalent alternative way of evaluating the resonant contribution is to use Eq. (2), the expression for the nonresonant case (Case III), in the integral over the spectral distribution. The pole in Eq. (2) is handled by taking the Cauchy principal value of the integral. This yields the same result for Case IV. This achieves a considerable simplification of the calculation, because a single expression can be used for both resonant and nonresonant contributions. Details can be

found in Appendix A.

In this work we neglect radiative damping and treat energy levels as arbitrarily sharp. This is a reasonable procedure because the typical radiative linewidths are much less than either the characteristic BBR frequency or the relevant atomic intervals.

The total shift can be calculated by integrating the contributions to the shift over the source spectrum. We then have a perturbation,

$$V_{ab}(\omega) = \langle a | e\vec{r} \cdot \vec{E}(\omega) | b \rangle / \hbar, \quad (3)$$

and a shift,

$$\delta\omega_a = \frac{e^2}{4\hbar^2} \sum_{i,b} |\langle a | r_i | b \rangle|^2 \times \int_0^\infty E_i^2(\omega) \left(\frac{1}{\omega_a - \omega_b - \omega} + \frac{1}{\omega_a - \omega_b + \omega} \right) d\omega. \quad (4)$$

$$\delta\omega_a = \frac{2e^2}{3\pi\hbar c^3} \sum_{i,b} |\langle a | r_i | b \rangle|^2 \int_0^\infty \omega^3 (e^{\hbar\omega/kT} - 1)^{-1} \left(\frac{1}{\omega_a - \omega_b - \omega} + \frac{1}{\omega_a - \omega_b + \omega} \right) d\omega. \quad (7)$$

We can express the matrix elements in terms of the Bohr radius a_0 and recast the integral in dimensionless form:

$$\delta\omega_a = \frac{2e^2}{3\pi\hbar c^3} a_0^2 \left(\frac{kT}{\hbar} \right)^3 \sum_{i,b} \left| \langle a | \frac{r_i}{a_0} | b \rangle \right|^2 F \left(\frac{\hbar(\omega_a - \omega_b)}{kT} \right), \quad (8)$$

where F is given by

$$F(y) = \int_0^\infty \left(\frac{1}{y+x} + \frac{1}{y-x} \right) \frac{x^3 dx}{e^x - 1}, \quad (9)$$

and y is defined by

$$y = \frac{\hbar(\omega_a - \omega_b)}{kT}. \quad (10)$$

The dependence of the dynamic Stark shift on the blackbody spectral distribution is entirely contained in the function $F(y)$, which is a universal function applicable to all atoms: Only the argument depends on atomic parameters. We have evaluated $F(y)$ by numerical integration and tabulated the result. Technical details, including the numerical treatment of the singularity at $x=y$, are discussed in Appendix B. $F(y)$, which is an odd function of y , is displayed in Fig. 1. The function vanishes at the origin and at $y = 2.616$. From Fig. 1 we can deduce the sign of the contribution to the Stark shift made by intermediate states. Nearby states, which satisfy $|y| < 2.616$, attract the shifted state; i.e., perturbing states lying above (below) the shifted state make a positive (negative) contribution to the shift. In contrast, distant states repel the shifted state.

Here $E_i(\omega)$ is the component of the electric field at circular frequency ω along the direction \hat{z} . Since the blackbody radiation is isotropic, each component of the electric field is related to the spectral energy density $u(\omega, T)$ at temperature T by

$$\frac{1}{8\pi} E_i^2(\omega) = \frac{1}{3} u(\omega, T). \quad (5)$$

The spectral energy density $u(\omega, T)$ is given in turn by the BBR formula

$$u(\omega, T) = \frac{\hbar}{\pi^2 c^3} \frac{\omega^3}{e^{\hbar\omega/kT} - 1}. \quad (6)$$

Combining Eqs. (4), (5), and (6), we obtain

It is worth noting that a perturbing state that is degenerate with the perturbed state (i.e., $\omega_a = \omega_b$) makes no contribution to the shift. Hence our second-order perturbation treatment is valid when applied to hydrogen. As an aside, we note the contrast with the *static* Stark effect, where the second-order perturbative expression notoriously diverges for hydrogen.

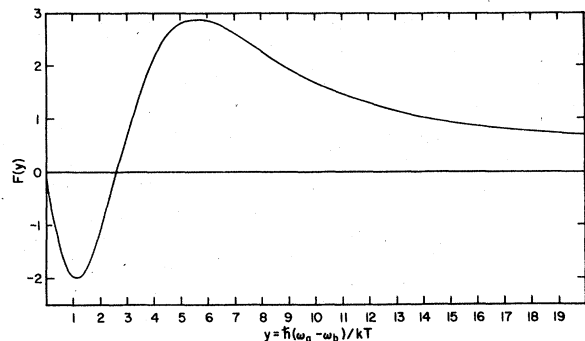


FIG. 1. The function $F(y)$ defined in Eqs. (8)–(10) in the text. Blackbody radiation causes a dynamic Stark shift in the energy ω_a of level a by an interaction with level b . The shift is proportional to $F(y)$, multiplied by the square of the electric-dipole matrix element. $F(y)$ is the integral of the off-resonant energy denominator over the spectral distribution of the blackbody radiation. We show the behavior for positive y ; for negative y , $F(-y) = -F(y)$. The sense of the interaction between states a and b is interesting: When states a and b are close in energy (small $|y|$), the states attract; when they are distant (large $|y|$), they repel.

For large and small values of the argument, $F(y)$ assumes the following asymptotic expressions:

$$F(y) \approx \begin{cases} -2y \int_0^\infty \frac{x dx}{e^x - 1} = -\frac{\pi^2 y}{3}, & |y| \ll 1 \\ \frac{2}{y} \int_0^\infty \frac{x^3 dx}{e^x - 1} + \frac{2}{y^3} \int_0^\infty \frac{x^5 dx}{e^x - 1} = \frac{2\pi^4}{15y} + \frac{16\pi^6}{63y^3}, & |y| \gg 1. \end{cases} \quad (11)$$

In evaluating Eqs. (11) and (12), we have used the definite integral²¹

$$\int_0^\infty \frac{x^{2n-1} dx}{e^x - 1} = (-1)^{n-1} \left(\frac{2\pi}{p}\right)^{2n} \frac{B_{2n}}{4n}, \quad (13)$$

where B_{2n} are the Bernoulli numbers.

The matrix element in Eq. (8) can be factored into radial and angular parts. Assuming LS coupling, we obtain

$$\left| \left\langle a \left| \frac{r_i}{a_0} \right| b \right\rangle \right|^2 = (R_{ab})^2 \left| \left\langle n_a L_a S_a J_a M_a \left| \frac{r_i}{r} \right| n_b L_b S_b J_b M_b \right\rangle \right|^2. \quad (14)$$

Here n is the principal quantum number, L is the orbital angular momentum, S is the spin, J is the total electronic angular momentum, and M is the z component of J . The dimensionless radial integral R_{ab} is given by

$$R_{ab} = \frac{1}{a_0} \int_0^\infty R_a(r) R_b(r) r^3 dr. \quad (15)$$

Here $R_a(r)$ and $R_b(r)$ are the radial parts of the atomic wave function.

We now sum Eq. (14) over all values of M_b and all three components i of r_i , deferring the sum over J_b for later. From standard angular momentum theory, we obtain an expression in terms of the reduced matrix element and the square of a $6-j$ symbol

$$\sum_{i, M_b} \left| \left\langle n_a L_a S_a J_a M_a \left| \frac{r_i}{r} \right| n_b L_b S_b J_b M_b \right\rangle \right|^2 = (2J_b + 1) \left\{ \begin{matrix} L_a & J_a & S_a \\ J_b & L_b & 1 \end{matrix} \right\}^2 |L_a \parallel \hat{n} \parallel L_b|^2. \quad (16)$$

Here \hat{n} represents the unit vector. The square of the reduced matrix element equals L_{\max} , the larger of L_a and L_b . Hence we rewrite Eq. (8) to express the shift in hertz, $\delta\nu_a = \delta\omega_a/2\pi$, as

$$\delta\nu_a = \frac{e^2}{3\pi^2 \hbar c^3} a_0^2 \left(\frac{kT}{\hbar}\right)^3 \sum_{n_b, L_b, J_b} (2J_b + 1) \left\{ \begin{matrix} L_a & J_a & S_a \\ J_b & L_b & 1 \end{matrix} \right\}^2 \times L_{\max} (R_{ab})^2 F\left(\frac{\hbar(\omega_a - \omega_b)}{kT}\right). \quad (17)$$

A simplification is possible when the perturbing states are energy degenerate with respect to J_b ; i.e., where, for fixed n_b and S_b , the variation of energy with J_b is much less than kT . In the degenerate case, for fixed n_b , we can neglect the variation of the function F with respect to J_b and sum over J_b in Eq. (17) using the sum rule for the $6-j$ symbols

$$\sum_{J_b} (2J_b + 1) \left\{ \begin{matrix} L_a & J_a & S_a \\ J_b & L_b & 1 \end{matrix} \right\}^2 = \frac{1}{2L_a + 1}. \quad (18)$$

Insertion of Eq. (18) into Eq. (17) then yields

$$\delta\nu_a = \frac{e^2}{3\pi^2 \hbar c^3} a_0^2 \left(\frac{kT}{\hbar}\right)^3 \sum_{n_b, L_b} \frac{L_{\max}}{2L_a + 1} (R_{ab})^2 F\left(\frac{\hbar(\omega_a - \omega_b)}{kT}\right). \quad (19)$$

Equations (17) and (19) are the expressions for the shift in the nondegenerate and degenerate cases, respectively.

We now derive an approximate expression valid for high values of n_a . If the bulk of the electric-dipole matrix element strength comes from states which satisfy $|\omega_a - \omega_b| \ll kT$, we may approximate $F(y)$ by its asymptotic expression for small $|y|$, Eq. (11). Substituting Eq. (11) in Eq. (8), we obtain the expression

$$\delta\omega_a \approx \frac{\pi e^2}{3m c^3} \left(\frac{kT}{\hbar}\right)^2 \left(\sum_{b,i} |\langle a | r_i | b \rangle|^2 (\omega_b - \omega_a) \frac{2m}{3\hbar} \right). \quad (20)$$

The summation in large parentheses is unity by the Thomas-Reiche-Kuhn sum rule,²² which applies to all atoms provided only that the states $|b\rangle$ satisfy completeness. We then obtain an expression for the shift $\delta\nu_a = \delta\omega_a/2\pi$:

$$\delta\nu_a = \frac{\alpha (kT)^2}{6\hbar m c^2}. \quad (21)$$

Here α is the fine-structure constant. At 300 K this expression evaluates to 2.417 kHz.

We can estimate the value of n for which Eq. (21) applies. As we will show below by explicit calculation, the largest contributions to the shift at room temperature typically come when $|n_b - n_a| \leq 1$. We want the corresponding atomic interval to be small enough so that Eq. (11) is usable. If we take $|y| < 0.5$, we obtain the condition

$$\hbar c R_\infty \left(\frac{1}{n^2} - \frac{1}{(n+1)^2} \right) \leq \frac{kT}{2}, \quad (22)$$

where R_∞ is the Rydberg constant in cm^{-1} . Since $n \gg 1$ this simplifies to

$$n \geq (4\hbar c R_\infty / kT)^{1/3}. \quad (23)$$

At $T = 300$ K this gives $n \geq 12.8$ as a rough value for the applicability of Eq. (21) and the onset of Rydberg behavior.

We should not, however, expect the results of an exact calculation to approach the value given by Eq. (21) asymptotically. To the extent that significant contributions come from states which do not satisfy $|y| \ll 1$, our use of Eq. (11) introduces error. A glance at Fig. 1 reveals that the curve is nonlinear [i.e., Eq. (11) overestimates the magnitude of $F(y)$] for $|y| \geq 0.5$. However, one cannot thereby conclude that Eq. (21) is an overestimate. Contributions of opposite sign are summed, and different contributions are affected differently by the use of Eq. (11).

Equation (21) predicts that the shift scales as T^2 in the limit where the major contributions to the shift satisfy $|y| < 1$. In the other limit, however, in which the major contributions come from states which satisfy $|y| > 1$, the scaling is different. Such a situation occurs for the 2S state of hydrogen, for example. $F(y)$, given approximately by Eq. (12), scales as T . If we neglect the variation of y in the sum indicated in Eq. (8), we obtain the result that the shift scales as T^4 .

B. Depopulation rates

We now consider the depopulation effect. BBR efficiently redistributes population among Rydberg states, shortens the atomic lifetime, and causes line broadening. The effective decay rate of a Rydberg state is then

$$\Gamma_{\text{eff}} = \Gamma_{\text{nr}} + \Gamma_{\text{BB}}, \quad (24)$$

where nr represents natural radiative decay. Our calculational approach, described below, is well suited only to the evaluation of the second (BBR-induced) term, for the following reasons. The principal contributions to the natural radiative decay rate come from transitions to low-lying states, whereas the principal contributions to the BBR-induced rate come from transitions to other Rydberg levels. Our calculations of the electric-dipole matrix elements are based on the Coulomb approximation,²³ which represents the wave function accurately for large values of r , but diverges for small values of r . Consequently, we know Rydberg-to-Rydberg matrix elements accurately and Rydberg-to-low-lying-state matrix elements inaccurately. We therefore have not calculated the natural radiative decay rate, but present instead the BBR-induced transition rate Γ_{BB} . The BBR-induced line broadening (in the absence of saturation effects) is then $\Gamma_{\text{BB}}/2\pi$. In the presence of saturation effects, one can still use the rates calculated here in a rate-equation approach, following the example of Lamb

and Sanders.²⁴

From Fermi's "Golden Rule" we have the transition rate to a final state b caused by a perturbation $\hat{V} \cos \omega t$:

$$\Gamma_{a \rightarrow b}^{\text{BB}}(\omega) = \frac{1}{2} \pi |V_{ab}|^2 \delta(\omega - \omega_{ab}). \quad (25)$$

Here $V_{ab}(\omega)$ is given by Eq. (3), and $\omega_{ab} = |\omega_a - \omega_b|$. Using Eq. (3) and integrating over ω , we obtain

$$\Gamma_{a \rightarrow b}^{\text{BB}} = \frac{\pi e^2}{2\hbar^2} \sum_i |\langle a | r_i | b \rangle|^2 E_i^2(\omega_{ab}). \quad (26)$$

Using Eqs. (5) and (6) and summing over all final states b , we obtain the total BBR-induced depopulation rate Γ_a^{BB} from state a

$$\begin{aligned} \Gamma_a^{\text{BB}} &= \sum_b \Gamma_{a \rightarrow b}^{\text{BB}} \\ &= \frac{4e^2}{3\hbar c^3} \sum_{i,b} |\langle a | r_i | b \rangle|^2 \frac{\omega_{ab}^3}{e^{\hbar\omega_{ab}/kT} - 1}. \end{aligned} \quad (27)$$

This expression can be rewritten as follows:

$$\Gamma_a^{\text{BB}} = \frac{4e^2}{3\hbar c^3} a_0^2 \left(\frac{kT}{\hbar}\right)^3 \sum_{i,b} \left| \left\langle a \left| \frac{r_i}{a_0} \right| b \right\rangle \right|^2 U(y). \quad (28)$$

Here

$$U(y) = |y|^3 (e^{|y|} - 1)^{-1} \quad (29)$$

and y is defined by Eq. (10) above. Evidently $U(y)$ is an even function of y . We now use Eqs. (14)–(16) to simplify the matrix elements. We obtain in the general case

$$\begin{aligned} \Gamma_a^{\text{BB}} &= \frac{4e^2}{3\hbar c^3} a_0^2 \left(\frac{kT}{\hbar}\right)^3 \sum_{n_b L_b J_b} (2J_b + 1) \left\{ \begin{matrix} L_a & J_a & S_a \\ J_b & L_b & 1 \end{matrix} \right\}^2 L_{\text{max}} \\ &\quad \times (R_{ab})^2 U(y). \end{aligned} \quad (30)$$

When the states with different values of J_b are degenerate in energy, we use Eq. (18) to perform the sum over J_b . We have then

$$\Gamma_a^{\text{BB}} = \frac{4e^2}{3\hbar c^3} a_0^2 \left(\frac{kT}{\hbar}\right)^3 \sum_{n_b L_b} \frac{L_{\text{max}}}{2L_a + 1} (R_{ab})^2 U(y). \quad (31)$$

Equations (30) and (31) give the depopulation rates in the nondegenerate and degenerate cases, respectively, corresponding to Eqs. (17) and (19) for the dynamic Stark shift.

For sufficiently high values of n_a , we obtain an approximate expression. Most of the electric-dipole matrix element strength occurs when $\hbar\omega_{ab} < kT$. We can expand the denominator in $U(y)$ to obtain

$$\Gamma_a^{\text{BB}} \simeq \frac{4e^2 a_0^2 kT}{3\hbar c^3} \sum_{n_b L_b} \frac{L_{\text{max}}}{2L_a + 1} (R_{ab})^2 \omega_{ab}^2. \quad (32)$$

We now apply the sum rule (Eq. 61.11 of Ref. 22)

$$\sum_{n_b} (R_{ab})^2 (\omega_{ab})^2 = \frac{4}{n_a^2} \left(\frac{e^2}{a_0 \hbar}\right)^2. \quad (33)$$

Equation (33) is valid only for hydrogen, but we can generalize to other atoms in the Coulomb approximation by using effective quantum numbers n^* in place of indicial quantum numbers n . After performing the sum over L_b in Eq. (32), we obtain

$$\Gamma_a^{\text{BB}} \cong \frac{4}{3} \left(\frac{e^2}{\hbar c} \right)^3 \left(\frac{kT}{\hbar} \right) \frac{1}{n_a^{*2}}. \quad (34)$$

At 300 K, this evaluates to $2.03 \times 10^7 (n_a^*)^{-2} \text{ sec}^{-1}$. This expression may be expected to apply when $|\omega_a - \omega_b| \lesssim kT/2$; i.e., for $n^* \gtrsim 12.8$, as discussed above.

Equation (34) is subject to a stronger caveat than that expressed above for the analogous Eq. (21). Contributions from states which do not satisfy $|y| \ll 1$ will be overestimated more severely by Eq. (34) than by Eq. (21), because of the extra factor of ω_{ab} in Eq. (32) compared to Eq. (20). Furthermore, since all the contributions to Eq. (32) are positive, no cancellation of errors can occur, contrary to the case of Eq. (20). Hence, Eq. (34) is definitely an overestimate.

C. Range of validity

In this section, we examine the possibility of a breakdown of our formalism at extreme values of n and T . We consider two topics: failure of the weak-field (perturbation) approximation, and breakdown of the electric-dipole approximation.

Taking up the first topic, we seek an appropriate criterion by which to judge the strength of the perturbing electric field, and thereby divide the weak-field and strong-field regimes. A number of different criteria have been proposed, each yielding different results. A recent review article by Bayfield²⁵ uses as a field-strength parameter the ratio of the excursion of a free electron in the perturbing electric field at frequency ω , $eE/m\omega^2$, to the radius of the Bohr orbit, $a_0 n^2$. We take the rms value of the BBR electric field, calculated from

$$\begin{aligned} E_{\text{rms}}^2 &= 8\pi \int_0^\infty \hbar \pi^{-2} c^{-3} \omega^3 \left[\exp\left(\frac{\hbar\omega}{kT}\right) - 1 \right]^{-1} d\omega \\ &= 8\pi^3 (kT)^4 / 15 (c\hbar)^3. \end{aligned} \quad (35)$$

Inserting the peak value of $\omega \sim 3kT/\hbar$, we obtain a value for the excursion of $1.48 \times 10^{-12} \text{ cm}$. The excursion is independent of T , because both E and ω^2 scale as T^2 , a peculiarity of the BBR spectrum. The radius of the Bohr orbit, $a_0 n^2 = 5 \times 10^{-9} n^2 \text{ cm}$, is much larger than the excursion for all values of n . In fact, the field-strength parameter actually decreases as n increases. This seems intuitively unreasonable and suggests

that this particular field-strength parameter is inappropriate.

Bayfield²⁵ also uses a second parameter for judging the electric-field strength, the ratio of the peak kinetic energy of a free electron, $e^2 E^2 / 2m\omega^2$, to the Coulomb binding energy $\alpha^2 m c^2 / 2n^2$. One obtains the ratio $W_{\text{osc}} / W_{\text{Coul}} = 7 \times 10^{-18} n^2 T^2$, where T is in degrees K. This ratio is much less than unity; equality is obtained only when $nT \sim 4 \times 10^8 \text{ K}$. Evidently this limit is not of practical interest.

We now consider a third way of judging the electric-field strength. When the blackbody radiation is sufficiently intense, the interaction of the Rydberg electron with the blackbody electric field is comparable to the interaction with the ionic core. That is,

$$en^2 a_0 E \sim \frac{1}{2} \alpha^2 m c^2 / n^2.$$

The rms electric field E can be evaluated using Eq. (35). The threshold condition is then

$$\left(\frac{8\pi^3}{15} \right)^{1/2} (kT)^2 n^2 \frac{\alpha^{-1/2}}{m c^2} \sim \frac{1}{2} \alpha^2 \frac{m c^2}{n^2}$$

or

$$kT \sim \left(\frac{15}{32\pi^3} \right)^{1/4} \alpha^{5/4} \frac{m c^2}{n^2}.$$

For $T = 300 \text{ K}$, the two interactions are of comparable magnitude for $n \sim 122$. For $n = 30$, this occurs at $T \sim 5000 \text{ K}$. When n and T are sufficiently high to be in the "strong BBR" regime, multiphoton processes will start to become important. An arbitrarily weak probe field interacting with the BBR-atom system will then induce complicated resonance line shapes. The concept of a simply defined dynamic Stark shift then becomes problematical.

We conclude the topic of strong perturbing electric fields by mentioning briefly two final strong-field effects. These effects turn out to be important only at extremely high values of n and T .

First, the dynamic Stark shift will ultimately become comparable to the spacing between n manifolds. Using Eq. (21) for the shift, and $\alpha^2 m c^2 / n^3$ for the level spacing between n manifolds, we put

$$\frac{\alpha (kT)^2}{6 m c^2} \sim \alpha^2 \frac{m c^2}{n^3}.$$

This yields $n \sim 2.6 \times 10^4$ at $T = 300 \text{ K}$. Such states can hardly be studied in the laboratory, since the Bohr radius $a_0 n^2$ for such a state is 3.4 cm .

The other conceivable limit arises from the BBR-induced transition rate. As the temperature increases, high-Rydberg levels are coupled more and more strongly into the continuum. The energy

levels are broadened until ultimately the width of the energy levels exceeds the spacing between levels. At this point discrete levels do not exist. Using Eq. (34) for the transition rate, we obtain

$$\frac{1}{2\pi} \frac{4}{3} \alpha^3 \frac{kT}{\hbar} \frac{1}{n^2} \sim \alpha^2 mc^2/n^3,$$

or

$$Tn \sim 3.8 \times 10^{12} \text{ K}.$$

We can safely confess to a lack of laboratory interest in this limit.

The final topic in this section is the possible breakdown of the electric-dipole approximation for the interaction between the atom and the radiation field. In this paper, we have assumed that the spatial variation of the BBR electric field over the atomic volume can be neglected. Mathematically, we have $k_{\text{rad}}r \ll 1$, where k_{rad} is the wave number of the radiation and r is the atomic radius. In this limit, we can make the approximation $\exp(\pm ik_{\text{rad}}r) \sim 1$. Evidently, higher-order terms will enter when $k_{\text{rad}}r \sim 1$. Taking k_{rad} to be its value at the peak of the BBR spectrum, $\sim 3kT/\hbar c$, and using the Bohr radius $r = a_0 n^2$, we obtain the condition for the breakdown of the electric-dipole approximation $kTn^2 \sim \alpha^2 mc^2/3$. At a temperature of 300 K, the indicated limit in n is $n \sim 219$; for $n = 30$, the limit in temperature is $T \sim 1.6 \times 10^4$ K. In the high- n , high- T regime, the higher-order multipoles of the radiation field may be comparable in effect to the electric-dipole approximation.

This conclusion seems superficially to contradict the well-known fact that the electric-dipole approximation continues to hold for Rydberg-to-Rydberg transitions as well as transitions among low-lying states. Because the radius of a Bohr atom scales as n^2 , while atomic energies scale as n^{-2} , the factor $k_{\text{rad}}r$ remains small for transitions among Rydberg states as well as low-lying states. The apparent contradiction disappears when we realize that the off-resonant dynamic Stark shift is an inherently different phenomenon from resonant transitions: The value of k_{rad} depends on the temperature, not on the atomic intervals.

To sum up: Only two ways of approaching the problem give limits which are likely to be realized in practice. At $T = 300$ K, the interaction of the Rydberg electron with the BBR electromagnetic field is comparable to the binding energy at $n \sim 122$, while the electric-dipole approximation breaks down at $n \sim 219$.

III. CALCULATION

The calculations were performed on a Nova 2/10 minicomputer (3%) and an Eclipse S/230 mini-

computer (97%), both from Data General Corporation, in double precision (16 decimal digits). Approximate total running time was 12 h on the Nova and 8 h on the Eclipse.

A. Evaluation of electric-dipole matrix elements

For hydrogen, we used the exact expressions in terms of confluent hypergeometric functions.²² The evaluation of the confluent hypergeometric functions involves the gamma function, which, for large values of quantum numbers, easily exceeds the 10^{475} dynamic range of the computer. Accordingly, one of us (W.H.W.) wrote a wide-ranging arithmetic software package to extend the dynamic range, allowing numbers in the range $10^{(4 \times 10^{16})}$ to be treated with 16-digit accuracy.

For helium and the alkalis, we used the following calculational techniques described by Zimmerman *et al.*²⁶ We used the Bates-Damgaard method,²³ based on the Coulomb approximation, for low values of the principal quantum number n . As n increased, the Bates-Damgaard calculation rapidly lost accuracy by the accumulation of round-off error. Consequently, for either the initial or final value of n greater than 15, the radial wave function was integrated directly using a Numerov algorithm whose source-code implementation was kindly supplied by Zimmerman. We tested these programs for possible coding errors by comparing the results with exact hydrogenic expressions and with existing Bates-Damgaard tables. The effect of spin-orbit interaction on the matrix elements was taken into account only through the binding energy (i.e., through n^*).

B. Summation over discrete perturbing states

In order to reproduce accurately the energies of a large number of atomic energy levels, we represented the energy by the quantum defect formula

$$E/\hbar c = -R/(n^*)^2 \equiv -R/(n - \delta)^2 \quad (36)$$

where R is the Rydberg constant (in cm^{-1}) for the atom.

$$\delta = \delta_0 + \delta_1 \left(\frac{1}{n - \delta_0} \right)^2 + \delta_2 \left(\frac{1}{n - \delta_0} \right)^4. \quad (37)$$

We performed least-squares fits to atomic energy levels to obtain optimized values for δ_0 , δ_1 , and δ_2 . Atomic energy-level data for the fit came from the work of Bashkin and Stoner²⁷ (Li, Na, K), Charlotte Moore²⁸ (Rb, Cs), and the authors²⁹ (He). For hydrogen we included the Lamb shift and relativistic corrections to order α^2 . For all elements considered, our treatment of the energy included fine structure and the reduced-mass cor-

rection, but neglected hyperfine structure. When performing the calculation, in certain cases we neglected the relativistic fine structure because its effect was negligible. Those cases are noted in the appropriate tables.

In order to perform the sum over the infinite number of discrete states, we made use of series regularities which obtain for large values of the principal quantum numbers n_a and n_b . The asymptotic behavior of the dipole matrix elements was then used to extrapolate to the ionization limit.

The sum over the perturbing states n_b was performed in three parts, according to the value of n_b . In the low- n regime, we calculated the contributions of individual states until the contributions had fallen off significantly. Typically the cutoff was $n_b = n_a + 10$, the largest contributions coming from $n_b \sim n_a$. Next, in the "intermediate- n regime," we calculated every tenth state and interpolated as described below, thus obtaining contributions up to some high $n_b \equiv N$ (typically $N = 50$). Finally, in the high- n regime, we estimated analytically the small residual contribution from all states with $n_b > N$.

In the intermediate- n regime of hydrogen, we used a simple formula to model the dependence of the matrix elements $(R_{ab})^2$ on n_b for fixed n_a . For a fixed value of n_a , we found empirically that the quantity

$$C(n_b) = (R_{ab})^2 n_b (n_b - n_a)^2 \quad (38)$$

varies much more slowly with n_b than does $(R_{ab})^2$. For example, for $n_a = 20$, when n_b varies from 30 to 90, $(R_{ab})^2$ varies by over two orders of magnitude, whereas $C(n_b)$ varies by only 20%. We also found that $C(n_b)$ varies more slowly with n_b than does the expression $(R_{ab})^2 n_b^3$.

In our calculation, we included a linear variation of $C(n_b)$ with n_b . In this approximation, $C(n_b)$ is given by

$$C(n_b) = C(n_1)(n_2 - n_b)/(n_2 - n_1) + C(n_2)(n_b - n_1)/(n_2 - n_1), \quad (39)$$

where n_1 and n_2 are two specific values of n_b for which the explicit evaluation of R_{ab} is performed. $(R_{ab})^2$ is then given for n_b by Eq. (38).

When $n_1 < n_b < n_2$, and $n_2 - n_1$ is not too large, this interpolation procedure yields accurate results. It is exact at the end points n_1 and n_2 . The only source of inaccuracy in $(R_{ab})^2$ is the assumption of linearity in Eq. (39).

When performing the sum, the function F was evaluated explicitly for each individual term. The evaluation of the contribution of the intermediate- n regime is probably accurate to a few percent at worst, because even the cruder approximation,

Eq. (38), with $C(n_b) = \text{constant}$, would be correct to ~20%, as mentioned above. Our level of accuracy is quite satisfactory, because the contribution of the entire intermediate- n region to the total shift is rather small. For the 15D state of hydrogen, for example, the intermediate- n region contributed 2% of the total dynamic Stark shift.

In addition, we remark on the behavior of very high Rydberg states ($n_b > N$). At large values of the principal quantum number n_b , the sum over perturbing states can be replaced by an integral over the binding energy E of the perturbing state. We obtain

$$\sum_{n_b} (R_{ab})^2 F\left(\frac{\hbar(\omega_a - \omega_b)}{kT}\right) \rightarrow \int (R_{ab})^2 F\left(\frac{\hbar(\omega_a - \omega_b)}{kT}\right) \rho(E) dE. \quad (40)$$

In Eq. (40), $\rho(E)$ represents the density of perturbing states and E is the binding energy of the perturbing state, given by Eq. (36). Therefore $\rho(E) = |dn_b^*/dE|$ is given by

$$\rho(E) = R^{1/2}/2 |E|^{3/2}. \quad (41)$$

The electric-dipole matrix element R_{ab} , defined in Eq. (15), represents the operator r evaluated between the radial wave functions for state a and state b . For sufficiently large values of the principal quantum number n_b of state b , $(R_{ab})^2$ falls off smoothly as $(n_b)^{-3}$ or $|E|^{3/2}$. This can be obtained in Eq. (38) when $n_b/n_a \gg 1$.

In Eq. (40), as n_b increases, E approaches zero. The decrease in the squared matrix element cancels the increase in the density of states $\rho(E)$. If we neglect the relatively slow dependence of F on energy, we then obtain the interesting result that equal energy intervals contribute equally to the shift in the very-high-Rydberg limit.

In our calculation, we estimated the small contribution from the infinite number of very-high-Rydberg states by refining the previous remark. We assumed that Eq. (38) gives the falloff of R_{ab} with n_b . We then used the integral³⁰

$$\int_{n_b}^{\infty} \frac{dn}{n(n-n_a)^2} = \frac{1}{n_a(n_b-n_a)} + \frac{1}{n_a^2} \ln\left(\frac{n_b-n_a}{n_b}\right). \quad (42)$$

For $n_b/n_a \gg 1$, this expression approaches $1/(2n_b^2)$. We took into account the variation of F over the asymptotic region by replacing F with its mean value, averaged with respect to the binding energy of the asymptotic region. This is the appropriate average because all energy intervals contribute equally in the limit of constant F .

The evaluation of the depopulation rate proceeds in an exactly analogous way. We perform the indicated sum in Eqs. (30) or (31) over all discrete perturbing states.

C. Contribution of continuum states

Accurate calculation of oscillator strengths of transitions between bound states and the continuum is quite difficult,³¹ except for some special cases, such as the ground state of hydrogen, for which a closed-form expression exists.²² Burgess and Seaton gave a semiempirical calculational method^{32,33} similar in spirit to the Bates and Damgaard²³ approach to transitions between bound states. The work of Burgess and Seaton was later revised and corrected by Peach.³⁴ The idea of the calculation is to use the quantum defects of the Rydberg states to obtain the phase shift in the continuum. This approach yields matrix elements as a function of the energy of the continuum state. For our purposes, one would have to integrate over the continuum energy. This is likely to yield significant error because the Burgess-Seaton method is accurate only for small positive values of the energy of the continuum state.³²

For this reason, and because the continuum correction is a small contribution in any event, we have chosen another method to estimate its size. We use a sum rule, valid for hydrogen [Eq. (61.7) of Ref. 22]:

$$\sum_{n_b} (R_{ab})^2 = \frac{1}{2} n_a^2 [5n_a^2 + 1 - 3L_a(L_a + 1)]. \quad (43)$$

The sum over n_b includes the continuum implicitly.

To estimate the continuum contribution to $(R_{ab})^2$, we summed the matrix elements over all discrete states using the method of the previous section, and attributed the remainder to the continuum using Eq. (43), appropriately generalized by using the effective quantum number n^* instead of n .

When calculating the continuum contribution to the shift, we used the value which F assumes at the ionization limit; i.e., we took $\omega_b = 0$. Similarly, when calculating the continuum contribution to the broadening, we used the blackbody spectral density at the ionization limit. This is tantamount to neglecting the variation of F over the continuum, or, equivalently, to assuming that the entire continuum contribution is made at the ionization limit. This method saved enormous amounts of computation and was warranted in view of the small size of the continuum contribution. For the 15P state of hydrogen, for example, the continuum contributes 0.4% of the total dynamic Stark shift and 0.09% of the total line-broadening effect.

D. Estimate of overall accuracy

The sum rule, Eq. (43), can be used to obtain an estimate of the overall accuracy. The continuum contribution calculated in the previous section turned out in some cases to have the wrong sign.

This indicates that the sum over discrete states of the squared electric-dipole matrix elements exceeded the value given in Eq. (43). If we assume the validity of Eq. (43), the "continuum contribution" then represents, in part, a first-order correction for this small effect, in addition to the actual contribution from the continuum states.

The situation is complicated by the fact that, in alkalis, the sum of oscillator strengths typically deviates³⁵ from the value given by the Thomas-Reiche-Kuhn sum rule by a few percent. The use of Eq. (43) may therefore actually introduce error into the calculation. In either event, we may take the typical size of the "wrong-sign" continuum contribution as indicative of the level of accuracy. A survey of the magnitude of this effect suggests that the accuracy is approximately 1% for non-hydrogenic elements, and up to an order of magnitude better for hydrogen. Other possible sources of error are estimated to be smaller: the evaluation of $F(y)$, the evaluation of electric-dipole matrix elements,²⁶ and the use of Eq. (38).

Additional evidence for the accuracy of the calculation is provided by the results of the calculation for high- n , high- L states of hydrogen. As discussed below, the result of the calculation of the dynamic Stark shift for the $n=30$, $L=29$ state of hydrogen agrees with the asymptotic formula within 0.13%.

IV. RESULTS

A. Dynamic Stark shifts at 300 K

1. Hydrogen

We take the 15D state of hydrogen as a "typical" Rydberg state bathed in BBR at 300 K. The contributions to the dynamic Stark shift of the energy of state a from different perturbing states b are shown in Fig. 2 as a function of the principal quantum number n_b . The largest contributions come from the $n=14$, 16, and 17 states, while the contributions from the $n=15$ states are negligible. Nearby states attract the perturbed state; i.e., states with $n < 15$ and $n > 15$ make, respectively, negative and positive contributions. Distant perturbing states ($n \leq 10$), make contributions of the opposite sign; i.e., they repel the shifted states. These contributions to the shift are much smaller (less than 5 Hz) and are not shown in Fig. 2. The sum of contributions from only the states with $14 \leq n_b \leq 17$ is 1791 Hz, or 90% of the sum of all contributions. The rapid falloff of contributions outside the region where $n_b \approx n_a$ results "primarily" from the falloff of the electric-dipole matrix elements; the variation of $F(y)$ is much slower. Typically the largest single contribution comes from $L_b = L_a + 1$, $n_b = n_a + 1$.

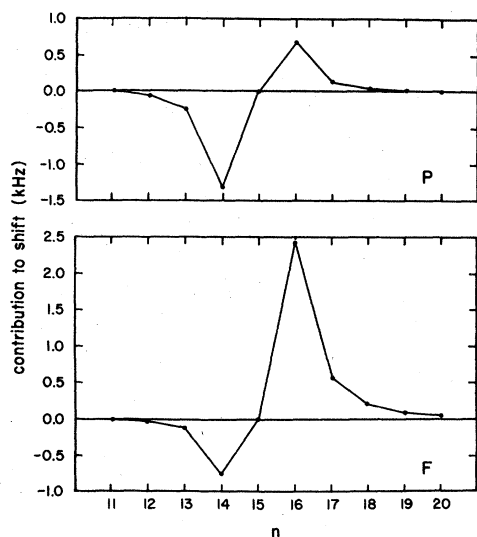


FIG. 2. Major contributions to dynamic Stark shift of energy level of $15D$ state of hydrogen induced by 300 K blackbody radiation. Contributions from various perturbing P and F states are displayed. Total shift is a sum of contributions from all perturbing states.

For comparison, Fig. 3 shows the contributions to the dynamic Stark shift of the energy of the $15D$ states of lithium, sodium, and potassium. Figure 4 shows the contributions to the shift of the $16D$ state of rubidium and the $17D$ state of cesium. We

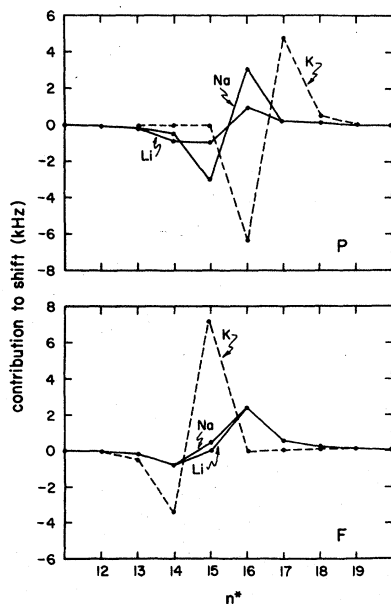


FIG. 3. Major contributions to dynamic Stark shift of energy level of $15D$ states of lithium, sodium, and potassium induced by 300 K blackbody radiation. In contrast to the case of hydrogen (Fig. 2), the contributions from $n = 15$ states do not vanish.

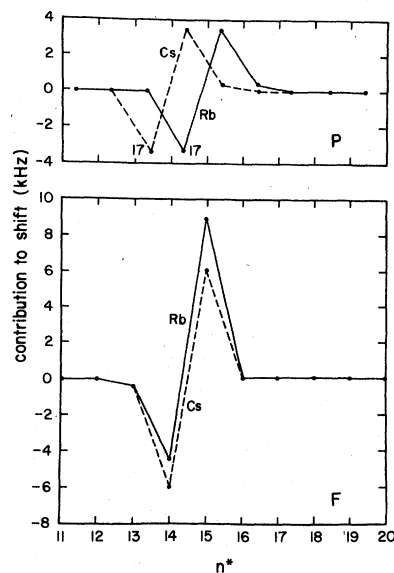


FIG. 4. Major contributions to the dynamic Stark shift of the energy levels of the $16D$ state of rubidium and the $17D$ state of cesium, which have $n^* \approx 15$. Temperature is 300 K.

made this choice of quantum numbers n in order to have n^* as close as possible to 15. The curves for the alkalis are qualitatively similar to the curves for hydrogen. The most important difference is that the contribution from $n_b = n_a$ does not vanish in alkali atoms because the states are not degenerate.

Summing all the contributions to the dynamic Stark shift, we obtained the total shift given by Eq. (19). The results for the nS states of hydrogen at 300 K are shown as a function of n in Fig. 5. The results for P , D , and F states are very similar; numerical results for S , P , D , and F states are listed in Table I. The shift is negative for small n (< 7), positive for $n \geq 8$, and approaches a limiting value for high n . The value of 2.417

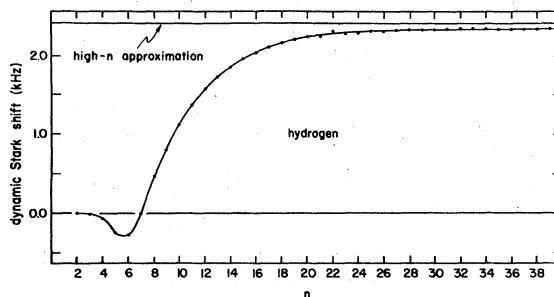


FIG. 5. Dynamic Stark shifts of energy levels of hydrogen S states induced by 300 K blackbody radiation. Also shown is an approximate formula, Eq. (21), applicable for high n .

TABLE I. Blackbody-radiation-induced dynamic Stark shifts (Hz) of energy levels of hydrogen at 300 K. Fine structure and the Lamb shift were neglected in performing the calculation.

n	${}^2S_{1/2}$	${}^2P_{1/2,3/2}$	${}^2D_{3/2,5/2}$	${}^2F_{5/2,7/2}$
1	-0.04128			
2	-1.077	-1.535		
3	-9.103	-11.51	-16.60	
4	-51.19	-60.37	-79.36	-108.15
5	-209.5	-235.6	-288.8	-369.37
6	-274.7	-291.5	-323.0	-362.27
7	1.344	15.60	48.57	111.54
8	393.9	424.8	490.3	599.07
9	761.1	797.1	870.9	987.45
10	1073	1108	1180	1289
11	1327	1360	1425	1523
12	1533	1563	1620	1705
13	1697	1723	1774	1846
14	1829	1850	1894	1956
15	1943	1947	1981	2036

kHz predicted by Eq. (21) is also shown in Fig. 5; it is an overestimate by $\approx 4\%$ of the actual limiting value.

The weak L dependence of the shift is shown in Fig. 6 for $n=30$. The shift approaches the value given by Eq. (21) more closely for high L . When $L=29$, the shift (2.424 kHz) agrees with the high- n approximation within 0.13%.

2. Helium

The dynamic Stark shifts for helium at 300 K are listed in Table II and displayed in Figs. 7 and 8. The curves for non-S states of helium more closely resemble the curves for hydrogen than do the S states. This is not surprising in view of the small quantum defects of the non-S states of helium.

3. Alkalis

Calculated dynamic Stark shifts induced by 300 K BBR are listed in Tables III-VII for alkali-metal atoms. These data are also displayed in

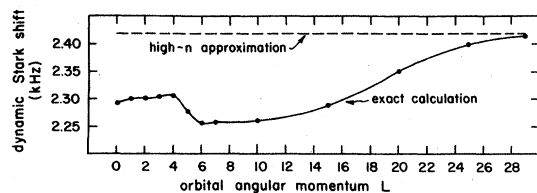


FIG. 6. Dynamic Stark shifts (kHz) in $n=30$ states of hydrogen induced by 300 K blackbody radiation. Also shown is an approximate formula, (Eq. 21), applicable for high n .

TABLE II. Effective quantum numbers n^* and blackbody-radiation-induced dynamic Stark shifts $\delta\nu$ (Hz) of energy levels of helium at 300 K. Singlet-triplet mixing was taken into account in performing the calculation only through its effect on n^* .

n	n^*	$\delta\nu$	1S	n^*	$\delta\nu$	3S	n^*	$\delta\nu$	1P	n^*	$\delta\nu$	3P	n^*	$\delta\nu$	1D	n^*	$\delta\nu$	3D	n^*	$\delta\nu$	1F	n^*	$\delta\nu$	3F	n^*	$\delta\nu$	1G	
1	0.86	-0.16																										
2	1.860	-7.6	1.703	2.012	0.738	1.932	1.932	17.58																				
3	2.860	-200.9	2.703	3.012	6.471	2.932	2.932	377.4																				
4	3.860	-8.97	3.703	4.012	-176.7	3.932	3.932	156.3																				
5	4.860	1173	4.703	5.012	-859.4	4.932	4.932	-255.4																				
6	5.860	2427	5.703	6.012	-1364	5.932	5.932	-210.4																				
7	6.860	3332	6.703	7.012	-1253	6.932	6.932	91.25																				
8	7.860	3681	7.703	8.012	-815.0	7.932	7.932	450.4																				
9	8.860	3619	8.703	9.012	-314.9	8.932	8.932	766.1																				
10	9.860	3487	9.703	10.012	146.9	9.932	9.932	1042																				
11	10.860	3410	10.703	11.012	542.5	10.932	10.932	1277																				
12	11.860	3271	11.703	12.012	852.5	11.932	11.932	1483																				
13	12.860	3154	12.703	13.012	1127	12.932	12.932	1633																				
14	13.860	3057	13.703	14.012	1348	13.932	13.932	1808																				
15	14.860	2917	14.703	15.012	1525	14.932	14.932	2151																				
20	19.860	2724	19.703	20.012	1985	19.932	19.932	2229																				
25	24.860	2544	24.703	25.012	2153	24.932	24.932	2288																				
30	29.860	2509	29.703	30.012	2227	29.932	29.932	2288																				

^aFine structure neglected in calculating shift of this energy level.

TABLE III. Effective quantum numbers n^* and blackbody-radiation-induced dynamic Stark shifts (Hz) of energy levels of lithium at 300 K. Fine structure was neglected in performing these calculations.

n	S			P			D		
	n^*	$\delta\nu$		n^*	$\delta\nu$		n^*	$\delta\nu$	
2	1.588 47	-1.43		1.9593	-1.145				
3	2.596 1	-38.62		2.9555	50.80		2.9985	-47.75	
4	3.598 2	-433.0		3.9542	292.9		3.9983	-219.2	
5	4.599 1	-454.1		4.9536	269.9		4.9982	-543.2	
6	5.599 6	1728		5.9532	-128.6		5.9982	-694.6	
7	6.599 8	3673		6.9530	-181.8		6.9982	-379.6	
8	7.600 0	4423		7.9529	58.15		7.9982	74.40	
9	8.600 1	4532		8.9528	375.3		8.9981	503.1	
10	9.600 2	4385		9.9528	691.0		9.9981	863.3	
11	10.600 3	4158		10.9527	973.9		10.9981	1156	
12	11.600 3	3929		11.9527	1217		11.9981	1393	
13	12.600 3	3721		12.9526	1426		12.9981	1584	
14	13.600 4	3555		13.9526	1601		13.9981	1738	
15	14.600 4	3408		14.9526	1756		14.9981	1865	
16	15.600 4	3410		15.9526	1799		15.9981	1946	
17	16.600 4	3253		16.9526	1895		16.9981	2015	
18	17.600 4	3128		17.9526	1970		17.9981	2073	
19	18.600 4	3032		18.9526	2074		18.9981	2116	
20	19.600 4	2813		19.9525	2112		19.9981	2147	
25	24.600 5	2661		24.9525	2211		24.9981	2233	
30	29.600 5	2602		29.9525	2280		29.9981	2278	

Figs. 9-13. The results permit a number of generalizations. At sufficiently high n , the dynamic Stark shift approaches a constant value, approximately given by Eq. (21). What is interesting

is the dependence on n and L of the shift before this limit is reached. In contrast to the hydrogenic case, the shift is strongly L dependent. The high- n limit is approached from above in

TABLE IV. Effective quantum numbers n^* and blackbody-radiation-induced dynamic Stark shifts (Hz) of energy levels of sodium at 300 K.

n	S			$P_{1/2}$		$P_{3/2}$		D		
	n^*	$\delta\nu$		n^*	$\delta\nu$	n^*	$\delta\nu$	n^*	$\delta\nu (D_{3/2})$	$\delta\nu (D_{5/2})$
3	1.627	-1.389		2.117	-2.985	2.1174	-2.998	2.990	-61.24	-61.25
4	2.643	-27.57		3.133	44.13	3.1133	43.94	3.988	15.73	14.46
5	3.647	-264.6		4.138	-254.8	4.1386	-253.7	4.987	279.8	279.7
6	4.649	-536.9		5.140	-1037	5.1410	-1037	5.986	784.6	786.7
7	5.650	616.2		6.141	-1511	6.1423	-1508	6.986	1351	1354
8	6.651	1660		7.142	-1453	7.1431	-1449	7.985	1698	1701
9	7.651	2178		8.143	-1060	8.1436	-1056	8.985	1902	1904
10	8.651	2421		9.143	-575.4	9.1439	-571.4	9.985	2029	2030
11	9.651	2528		10.143	-112.0	10.1441	-108.5	10.985	2115	2116
12	10.651	2571		11.144	295.6	11.1443	298.5	11.985	2202	2203
13	11.651	2585		12.144	608.0	12.1445	610.0	12.985	2257	2258
14	12.651	2590		13.144	918.0	13.1446	919.9	13.985	2322	2322
15	13.652	2582		14.144	1189	14.1447	1191	14.985	2393	2395
16	14.652	2585		15.144	1383 ^a	15.1447	1383 ^a	15.985	2374 ^a	2374 ^a
17	15.652	2564		16.144	1534 ^a	16.1448	1534 ^a	16.985	2385 ^a	2385 ^a
18	16.652	2539		17.144	1660 ^a	17.1448	1660 ^a	17.985	2391 ^a	2391 ^a
19	17.652	2697		18.144	1755 ^a	18.1449	1755 ^a	18.985	2393 ^a	2393 ^a
20	18.652	2508		19.144	1837 ^a	19.1449	1837 ^a	19.985	2393 ^a	2393 ^a
25	23.652	2468		24.144	2103 ^a	24.1450	2103 ^a	24.985	2366 ^a	2366 ^a
30	28.652	2472		29.144	2212 ^a	29.1451	2212 ^a	29.985	2378 ^a	2378 ^a

^aFine structure neglected in calculation of shift for this state.

TABLE V. Effective quantum numbers n^* and blackbody-radiation-induced dynamic Stark shifts (Hz) of energy levels of potassium at 300 K.

n	S		$P_{1/2}$		$P_{3/2}$		D		
	n^*	$\delta\nu$	n^*	$\delta\nu$	n^*	$\delta\nu$	n^*	$\delta\nu (D_{3/2})$	$\delta\nu (D_{5/2})$
3							2.854	-16.47	-16.30
4	1.770	-2.528	2.232	-5.370	2.235	-5.471	3.797	-171.9	-170.8
5	2.801	-45.76	2.263	-76.77	3.266	-78.97	4.770	357.3	358.7
6	3.810	-412.5	4.273	-42.71	4.276	-43.62	5.755	1293	1282
7	4.814	-429.8	5.278	87.31	5.281	107.3	6.746	1734	1715
8	5.816	1143	6.280	1167	6.283	1216	7.740	1676	1657
9	6.817	2284	7.282	1742	7.285	1798	8.736	1228	1211
10	7.818	2769	8.283	1807	8.286	1858	9.733	497.8	483.4
11	8.818	2941	9.283	1493	9.286	1536	10.731	-234.8	-246.6
12	9.818	2973	10.284	1006	10.287	1043	11.730	-585.2	-594.8
13	10.819	2947	11.284	623.2	11.287	653.9	12.728	-173.9	-181.7
14	11.819	2900	12.284	621.1	12.287	648.4	13.727	1703	1695
15	12.819	2852	13.285	1216	13.288	1241	14.727	3184	3178
16	13.819	2822	14.285	2651 ^a	14.288	2651 ^a	15.726	2525 ^a	2525 ^a
17	14.819	2780	15.285	2603 ^a	15.288	2603 ^a	16.726	2522 ^a	2522 ^a
18	15.819	2727	16.285	2549 ^a	16.288	2549 ^a	17.725	2447 ^a	2447 ^a
19	16.819	2862	17.285	2553 ^a	17.288	2553 ^a	18.725	2505 ^a	2505 ^a
20	17.819	2798	18.285	2564 ^a	18.288	2564 ^a	19.724	2502 ^a	2502 ^a
25	22.820	2533	23.285	2374 ^a	23.289	2374 ^a	24.723	2455 ^a	2455 ^a
30	27.820	2503	28.286	2359 ^a	28.289	2359 ^a	29.723	2465 ^a	2465 ^a

^aFine structure neglected in calculation of Stark shift for this state.

some cases and from below in others. For a given L , the shift as a function of n can change sign several times. Naively, one might expect to obtain valid results for alkalis by merely interpolating in the results for hydrogen, using n^* in-

stead of n . Evidently, this procedure would fail badly. Physically the reason is clear: The Stark shift in the energy of a state depends not only on the quantum defect of that state, but also on the quantum defects of the perturbing states.

TABLE VI. Effective quantum numbers n^* and blackbody-radiation-induced dynamic Stark shifts (Hz) of energy levels of rubidium at 300 K.

n	S		$P_{1/2}$		$P_{3/2}$		$D_{3/2}$		$D_{5/2}$	
	n^*	$\delta\nu$	n^*	$\delta\nu$	n^*	$\delta\nu$	n^*	$\delta\nu$	n^*	$\delta\nu$
4							2.767	-6.467	2.767	-6.975
5	1.805	-2.789	2.280	-7.511	2.293	-8.127	3.706	-188.7	3.707	-181.4
6	2.845	-48.17	3.317	-151.8	3.330	-166.6	4.683	71.28	4.684	66.51
7	3.856	-411.7	4.329	-484.5	4.342	-473.8	5.672	593.3	5.673	554.2
8	4.861	-386.7	5.335	836.6	5.348	938.6	6.666	1185	6.667	1147
9	5.863	1020	6.338	2372	6.351	2503	7.662	1586	7.664	1558
10	6.865	2004	7.339	3096	7.353	3217	8.660	1823	8.661	1805
11	7.866	2454	8.341	3318	8.354	3419	9.658	1932	9.659	1921
12	8.866	2646	9.342	3324	9.355	3406	10.657	1964	10.658	1956
13	9.867	2715	10.342	3247	10.355	3313	11.656	1969	11.657	1965
14	10.867	2727	11.343	3147	11.356	3201	12.655	2013	12.656	2009
15	11.867	2712	12.343	3054	12.356	3099	13.654	2152	13.656	2150
16	12.867	2688	13.343	3016	13.356	3051	14.654	2382	14.655	2381
17	13.868	2661	14.343	2915	14.357	2944	15.653	2434	15.655	2436
18	14.868	2641	15.344	2910	15.357	2929	16.653	2439	16.655	2441
19	15.868	2610	16.344	2816	16.357	2832	17.653	2441	17.655	2442
20	16.868	2576	17.344	2736	17.357	2807	18.653	2440	18.654	2442
25	21.868	2503	22.344	2461	22.357	2469	23.652	2419	23.654	2420
30	26.868	2477	27.344	2407	27.358	2412	28.652	2425	28.653	2425

TABLE VII. Effective quantum numbers n^* and blackbody-radiation-induced dynamic Stark shifts (Hz) of energy levels of cesium at 300 K.

n	S		$P_{1/2}$		$P_{3/2}$		$D_{3/2}$		$D_{5/2}$	
	n^*	$\delta\nu$	n^*	$\delta\nu$	n^*	$\delta\nu$	n^*	$\delta\nu$	n^*	$\delta\nu$
5							2.513	5.497	2.5550	5.315
6	1.869	-3.589	2.329	-14.85	2.362	-17.24	3.519	-70.41	3.536	-99.18
7	2.920	-59.67	3.374	-153.4	3.406	-111.7	4.522	-810.4	4.534	-825.8
8	3.934	-477.4	4.389	410.6	4.421	425.2	5.523	-409.6	5.534	-299.4
9	4.940	-291.7	5.396	1096	5.428	1049	6.524	738.2	6.534	929.2
10	5.943	1206	6.399	1498	6.432	1437	7.525	1594	7.534	1804
11	6.945	2174	7.402	1741	7.434	1671	8.525	2042	8.534	2239
12	7.946	2603	8.403	1905	8.435	1840	9.525	2172	9.535	2346
13	8.947	2779	9.404	2029	9.436	1973	10.526	2093	10.535	2231
14	9.947	2833	10.405	2120	10.437	2093	11.526	1908	11.535	2038
15	10.948	2828	11.405	2203	11.438	2146	12.526	1799	12.535	1903
16	11.948	2764	12.406	2246	12.438	2187	13.526	2604	13.535	2696
17	12.948	2733	13.406	2275	13.439	2223	14.526	2601	14.535	2678
18	13.949	2702	14.406	2291	14.439	2251	15.526	2581	15.535	2648
19	14.949	2676	15.407	2303	15.439	2269	16.526	2670	16.535	2724
20	15.949	2640	16.407	2311	16.439	2280	17.526	2627	17.535	2675
25	20.949	2531	21.407	2315	21.440	2296	22.526	2475	22.535	2502
30	25.949	2497	26.408	2305	26.440	2298	27.526	2431	27.536	2450

B. Depopulation rates at 300 K

1. Hydrogen

We return to our typical Rydberg state, the 15D state. Figure 14 shows the major contributions to the total depopulation rate from various perturbing states. The largest contributions come when $n_b \approx n_a$. All contributions are, of course, positive, because Eq. (30) is positive definite.

Summing all the contributions to the depopulation rate yields the total BBR-induced depopulation rate. The results for the S states of hydrogen are shown as a function of n in Fig. 15 and

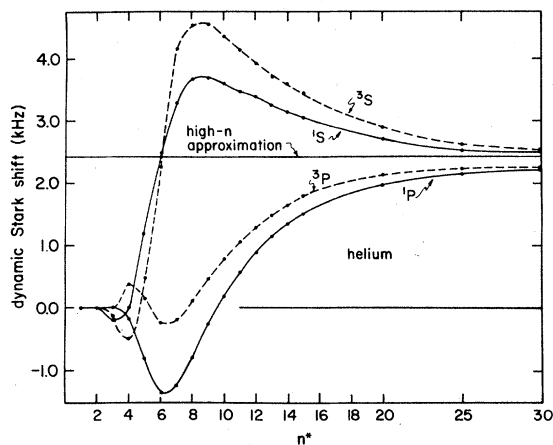


FIG. 7. Dynamic Stark shifts (kHz) of energy levels of Rydberg S and P states of helium induced by 300 K blackbody radiation.

listed in Table VIII. The results for the P, D, and F states are very similar and are also listed in Table VIII. The depopulation rate rises to a maximum of $36 \times 10^3 \text{ sec}^{-1}$ at $n=11$ and 12, and then decreases with n . Figure 15 also displays the high- n value given by Eq. (34). As discussed in Sec. II B above, this is an overestimate, and the approach to asymptotic behavior is not as rapid for the depopulation rate as is the case for the dynamic Stark shift.

The variation of the depopulation rate as a function of L for $n=30$ is shown in Fig. 16. The rate increases with L , approaching the value given by the high- n approximation for high L . The error in the high- n approximation decreases smoothly from 67% at $L=0$ to 2% at $L=29$.

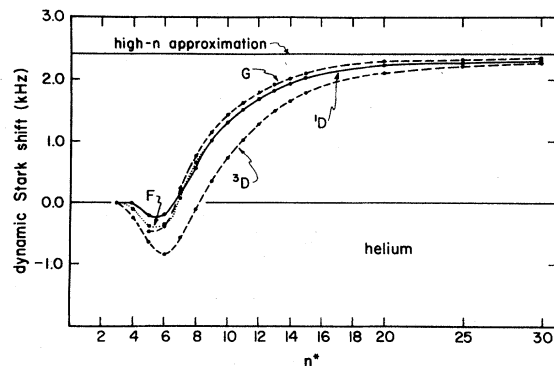


FIG. 8. Dynamic Stark shifts (kHz) of energy levels of Rydberg D, F, and G states of helium induced by 300 K blackbody radiation. For $n \geq 8$, the curve for F states overlaps the curve for 1D states.

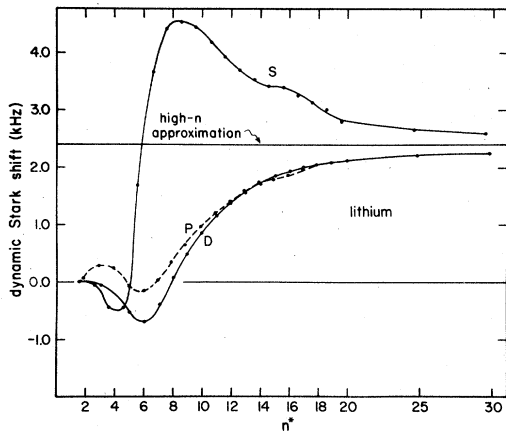


FIG. 9. Dynamic Stark shifts (kHz) of energy levels of lithium induced by 300 K blackbody radiation.

2. Helium and the alkalis

The depopulation rates for helium and the alkalis are displayed in Figs. 17–23 and listed in Tables IX–XIV. The depopulation rates all have the same general shape: a sharp threshold at $n \approx 7$, rising to a peak near $n \approx 12$, followed by a gradual decline. The maximum value is typically $\approx 10^5 \text{ sec}^{-1}$. The high- n approximation is an overestimate, but its accuracy increases with n .

C. Hydrogen at other temperatures

As the ambient temperature increases, the magnitudes of both effects increase. The asymptotic value for the dynamic Stark shift, Eq. (21), increases as T^2 , while that for the depopulation rate varies as T . The approach to asymptotic behavior occurs at lower values of n_a ; the threshold given by Eq. (23) scales as $T^{-1/3}$. Figure 24 shows the dynamic Stark shift and Fig. 25 shows the depopulation rate, both for several states of

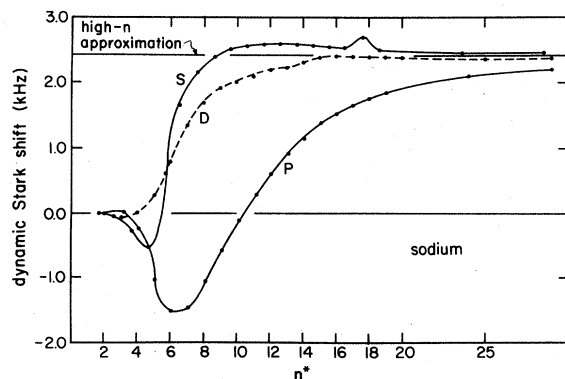


FIG. 10. Dynamic Stark shifts (kHz) of energy levels of sodium induced by 300 K blackbody radiation.

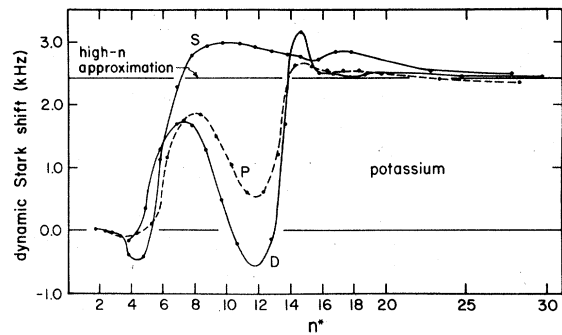


FIG. 11. Dynamic Stark shifts (kHz) of energy levels of potassium induced by 300 K blackbody radiation.

hydrogen over a wide range of temperatures. As discussed above, and shown in Fig. 24, the dynamic Stark shift scales as T^4 at low n , and as T^2 at high n . Figure 25 demonstrates that the depopulation rate scales roughly as T for high n . For low n , the rate increases much more rapidly because of the exponential factor in Eq. (29).

V. DISCUSSION

A. Comparison with other work

1. Dynamic Stark shift

Gallagher and Cooke¹ first presented an asymptotic formula for the dynamic Stark shift for sufficiently high Rydberg states. Their Eq. (7) corresponds to Eq. (21) of this work. The asymptotic formula gives the same result for all Rydberg states of all atomic species. In this early work, no attempt was made to perform accurate calculations of the Stark shift for individual states in any atomic species, as is done in the present work. Our work also corrects minor numerical factors in the earlier work. In Ref. 1, Eq. (6) omits a factor of $\frac{1}{2}$, and Eq. (7) omits a factor of π . References 1 and 3 contain a minor numerical error in evaluating the 300 K dynamic Stark shift in the

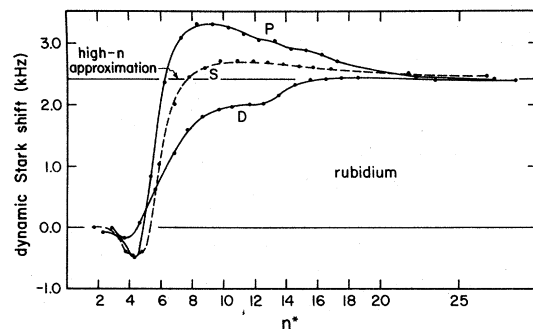


FIG. 12. Dynamic Stark shifts (kHz) of energy levels of rubidium induced by 300 K blackbody radiation.

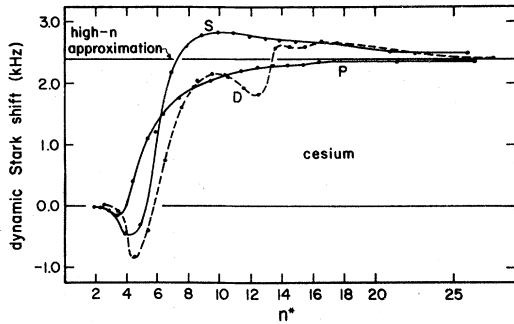


FIG. 13. Dynamic Stark shifts (kHz) of energy levels of cesium induced by 300 K blackbody radiation.

high- n limit, obtaining 2.2 kHz, compared to the correct result of 2.417 kHz.

There is another disagreement between the present work and Refs. 1 and 3 in explaining the fact that Rydberg states experience a larger dynamic Stark shift than do low-lying states. This effect is attributed in Refs. 1 and 3 to the relative magnitudes of the relevant atomic energy intervals. For Rydberg states, the atomic intervals making contributions to the Stark shift are less than kT , whereas for low-lying states, relevant intervals are comparable to or larger than kT . We can rewrite Eq. (7) to obtain

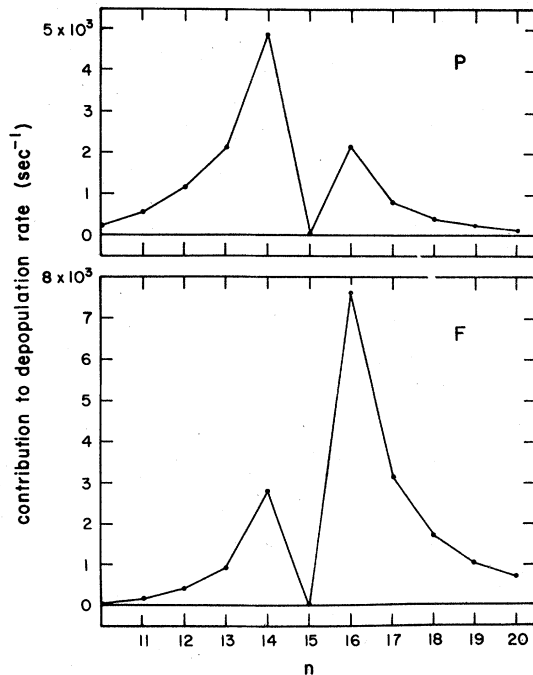


FIG. 14. Major contribution to blackbody-induced transition rates of 15D state of hydrogen at 300 K.

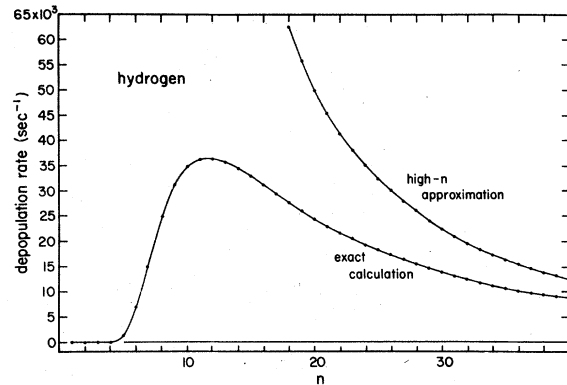


FIG. 15. Depopulation rates of Rydberg states of hydrogen caused by 300 K blackbody radiation. Also shown is an approximation, Eq. (34), which applies for high n (> 13).

$$\delta\omega_a = \frac{4e^2}{3\pi\hbar c^3} \sum_{i,b} |\langle a | r_i | b \rangle|^2 \int_0^\infty \omega^3 (e^{\hbar\omega/kT} - 1)^{-1} \times \left(\frac{\omega_{ab}}{\omega_{ab}^2 - \omega^2} \right) d\omega. \quad (44)$$

The influence of the relative size of the atomic interval is contained in the last factor in the integrand. When the atomic interval ω_{ab} is much less than the typical BBR frequency ω , the factor is approximately $-\omega_{ab}\omega^{-2}$. Since this factor decreases with the atomic interval ω_{ab} , this factor, taken by itself, would tend to produce smaller shifts in the high-lying states (where $\hbar\omega_{ab} \ll kT$) than in low-lying states (where $\hbar\omega_{ab} \sim kT$). The real explanation for the larger shifts in high-lying states is their larger electric-dipole matrix elements, which more than compensate for the smaller off-resonance factor.

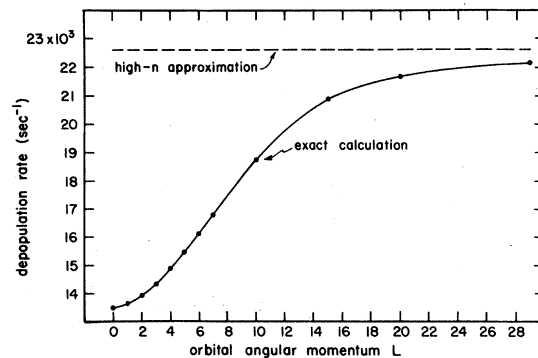


FIG. 16. Depopulation rates (sec^{-1}) of $n=30$ states of hydrogen induced by 300 K blackbody radiation. Also shown is an approximate formula, Eq. (34), applicable for high n .

TABLE VIII. Blackbody-radiation-induced depopulation rates (sec^{-1}) of states of hydrogen at 300 K. Fine structure and the Lamb shift were neglected in performing the calculation.

n	S	P	D	F
1	0.00			
2	1.42×10^{-5}	4.73×10^{-6}		
3	7.97×10^{-5}	4.33×10^{-4}	3.5×10^{-4}	
4	16.02	19.49	27.02	39.86
5	1199	1380	1762	2385
6	7038	7878	9618	12370
7	16520	18160	21500	26700
8	25360	27420	31580	37930
9	31370	33470	37690	44030
10	34680	36630	40526	46320
11	35970	37710	41150	46240
12	35930	37440	40430	44810
13	35060	36360	38920	42670
14	33700	34820	37010	40210
15	32150	33050	34920	37650

At present, there are no experimental data with which to compare the results of our calculations. However, the predicted size of the effect is within the reach of present laser technology. An experimental verification of the predictions would be most welcome.

2. Depopulation rates

Gallagher and Cooke^{1,5} and Cooke and Gallagher³ presented theoretical and experimental results on the depopulation rates from Rydberg states of sodium. In Ref. 1, theoretical calculated BBR-induced depopulation rates for the $17P$ and $18P$ states of sodium successfully accounted for the discrepancy in lifetimes between the experimentally measured lifetimes and the calculated natural radiative lifetimes.² In Table XV we compare our results with theirs. Agreement is satisfactory. Inconsistencies arise between this work and earlier work. Equations (2)–(4) of Ref. 1 appear to confuse the Einstein A coefficient with the Einstein B coefficient. The corresponding equations are Eqs. (25)–(31) in the present work.

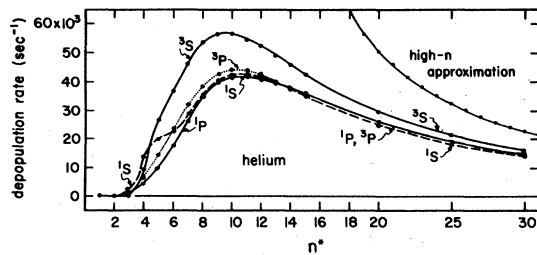


FIG. 17. Depopulation rates (sec^{-1}) of Rydberg S and P states of helium induced by 300 K blackbody radiation.

Also, Ref. 1 states that by far the most dramatic lifetime effect occurs for the high n P states. In fact, the high- L states will demonstrate an even larger effect, because the BBR-induced depopulation rate generally increases with L for fixed n , while the competing mechanism of radiative decay falls off with L (see Fig. 16).

B. Implications for high-precision spectroscopy

In a previous paper, we reported an extensive series of measurements of the fine structure of highly excited states of helium.²⁹ The experimental apparatus was described in a separate publication.³⁶ We considered the possibility of systematic effects from blackbody radiation, but neglected it after performing a preliminary calculation. Table XVI shows the calculated magnitude of the expected shift in the relevant helium Rydberg energy levels caused by a 300 K module and a 1400 K cathode, weighted by their respective solid angles. The cathode subtends an effective solid angle of 0.25 sr averaged over the interaction volume. The largest energy-level shift in Table XVI

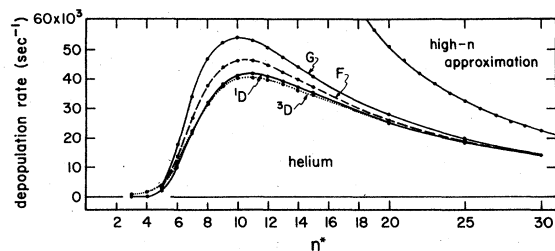


FIG. 18. Depopulation rates (sec^{-1}) of Rydberg D, F, and G states of helium induced by 300 K blackbody radiation.

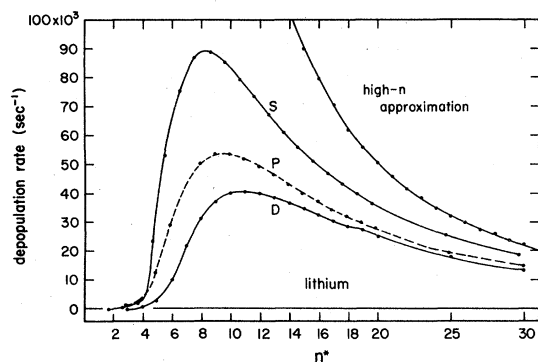


FIG. 19. Depopulation rates (sec^{-1}) of Rydberg states of lithium induced by 300 K blackbody radiation.

is about 2.6 kHz; the shifts in transition frequencies are smaller still. Since the smallest uncertainty reported in Ref. 29 was 50 kHz, our neglect of the BBR effects was justified.

The shift in a transition frequency is the difference between the shifts of the initial and final states; the shift itself is a strong function of n and a weak function of L . Hence the effect is minimal in transitions in which n does not change, such as the measurements reported in Ref. 29. Transitions in which n changes substantially, such as those studied in the work of Lee *et al.*³⁷ and Rosenbluh *et al.*,³⁸ will show a larger effect. Neither of these last two papers reported measurements of sufficient sensitivity to detect a BBR-induced shift.

We also have calculated the effect of BBR on two intervals of interest for fundamental constant remeasurement: the Lamb shift and the 1S-2S interval in hydrogen. The Lamb-shift experiment of Kaufman *et al.*³⁹ used a module similar in construction to ours, with a tungsten wire cathode.

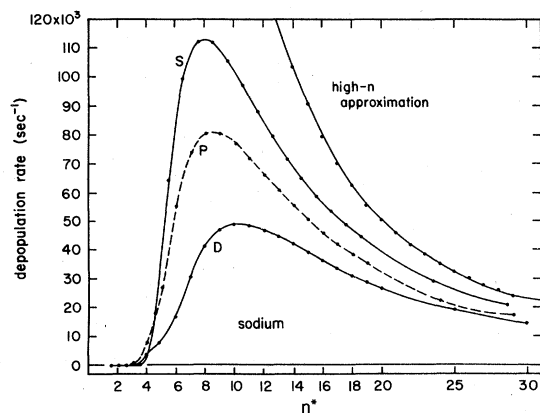


FIG. 20. Depopulation rates (sec^{-1}) of Rydberg states of sodium induced by 300 K blackbody radiation.

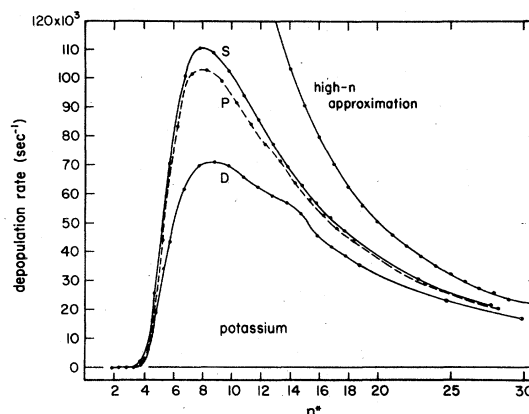


FIG. 21. Depopulation rates (sec^{-1}) of Rydberg states of potassium induced by 300 K blackbody radiation.

If we assign a solid angle of 0.25 sr to a 2500 K cathode, we obtain an effect of a mere 63 Hz. This could not account for the ≈ 200 kHz discrepancy between this result and the other Lamb-shift measurements. The effect of 300 K BBR on the hydrogen 1S-2S interval is to decrease the interval by 1.04 Hz. This is comparable to the natural radiative width of 1.31 Hz for this interval.⁴⁰

In the future, the line broadening effect may set a limit on linewidths attainable in precision experiments. The experimenter's answer is to cool the apparatus to cryogenic temperatures, as is already done for other reasons in the high-precision ion-trap work by Dehmelt and coworkers.⁴¹ An interesting point is that in the high- n approximation, Eq. (34), the BBR-induced depopulation rate decreases as n^{-2} , whereas the natural radiative decay rate for fixed L falls off as n^{-3} . Thus, ultimately, the blackbody rate dominates at high n . In sodium P states at 300 K, the two become

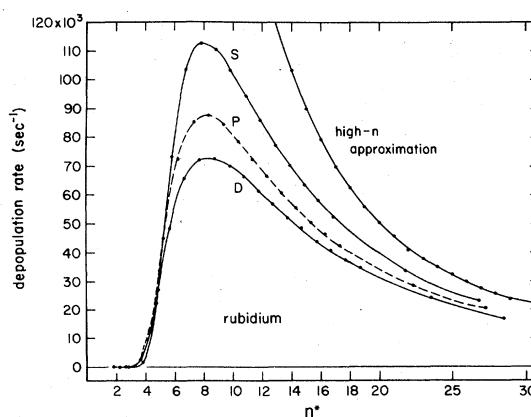


FIG. 22. Depopulation rates (sec^{-1}) of Rydberg states of rubidium induced by 300 K blackbody radiation.

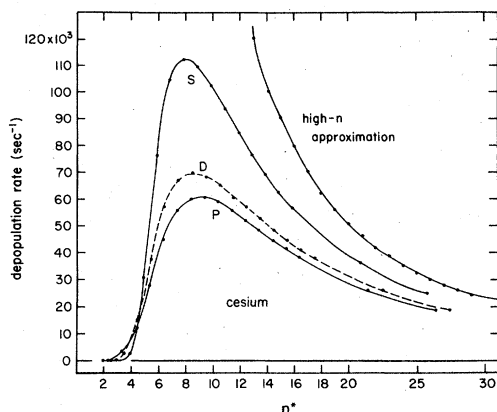


FIG. 23. Depopulation rates (sec^{-1}) of Rydberg states of cesium induced by 300 K blackbody radiation.

equal⁴² at $n=12$. When the transitions are saturated, the Rydberg states are strongly coupled into a degenerate "reservoir state," and the population of a given state exhibits nonexponential decay. In hydrogen at 2.84 K, the background radiation temperature of the universe,⁴³ equality of rates occurs at $n=39$, $L=38$. This result may have significant implications for analyses of conditions in interstellar media which are based on intensities of radio recombination lines, since those lines originate from levels having $n \geq 100$.

ACKNOWLEDGMENTS

This material is based upon work supported by the National Science Foundation under Grant No.

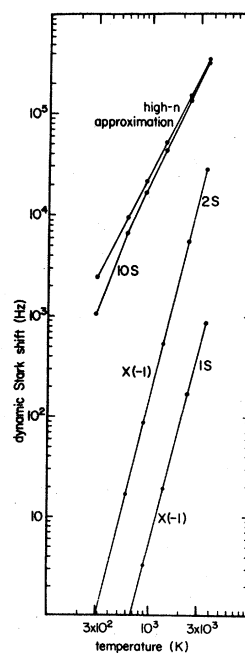


FIG. 24. Dynamic Stark shifts (kHz) of selected energy levels of hydrogen as a function of temperature.

PHY77-15217. One of us (J.W.F.) held a National Needs postdoctoral fellowship from the National Science Foundation during part of this work. We are grateful to Willis E. Lamb, Jr. for valuable discussions, to Ken Harvey and Michael Littman for useful comments, to Myron L. Zimmerman for giving us a preprint of Ref. 26 and a copy of his

TABLE IX. Blackbody-radiation-induced depopulation rates (sec^{-1}) of states of helium at 300 K. For values of n^* , see Table II.

n	$1S$	$3S$	$1P$	$3P$	$1D$	$3D$	$1F$	$3F$	$1,3G$
1	0.00								
2	1×10^{-3}	6×10^{-11}	4×10^{-4}	2×10^{-11}					
3	1271	60.43	687.7	1897	158.4	1126			
4	13260	8626	4702	6493	174.1	2185	40.9	42.0	
5	20040	26860	8953	14030	1831	3893	2378	2380	3307
6	22440	36670	17150	22670	9618	11450	12340	12330	16300
7	28930	46250	27290	31840	21610	22470	26640	26620	33920
8	36060	53670	35280	38900	31800	31780	37840	37820	46550
9	40580	56840	39950	42860	37960	37460	43950	43930	52460
10	42580	56910	41900	44280	40800	40110	46250	46220	53910
11	42770	55170	42000	43980	41420	40680	46180	46150	52830
12	41820	52500	40950	42640	40670	39950	44760	44740	50440
13	40210	49410	39240	40720	39150	38480	42630	42610	47460
14	38250	46220	37190	38520	37220	36610	40180	40160	44290
15	36150	43110	35020	36250	35120	34590	37640	37630	41130
20	26340	30000	25110	25800	25330	24950	26520	26510	28180
25	19390	21570	18300	18770	18660	18420	19110 ^a	19110 ^a	20010
30	14700	16120	13800	14140	14190	14030	14320 ^a	14320 ^a	14850

^a Fine structure neglected in calculating depopulation rate for this state.

TABLE X. Blackbody-radiation-induced depopulation rates (sec^{-1}) of states of lithium at 300 K. For values of n^* , see Table III.

n	S	P	D
2	1×10^{-23}	2.7×10^{-19}	
3	0.20	1442	864.9
4	2137	2810	1215
5	23720	12970	2848
6	53080	29580	10500
7	76510	42710	21800
8	87380	50270	31400
9	88640	53290	37260
10	85050	53370	40010
11	79420	51730	40630
12	73180	49190	39940
13	67010	46260	38480
14	61230	43200	36620
15	55970	40210	34590
16	51118	37290	32480
17	46820	34610	30450
18	42990	32130	28510
19	39560	29860	26690
20	36490	27790	24990
25	25270	19830	18210
30	18430	14820	13790

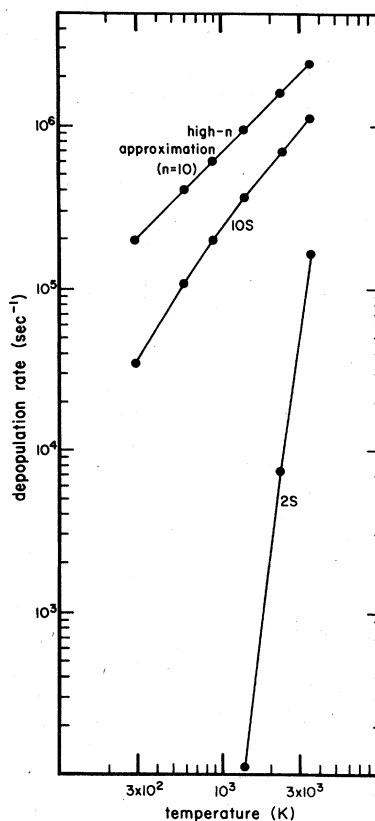


FIG. 25. Depopulation rates (sec^{-1}) of selected states of hydrogen as a function of temperature. Also shown is the high- n approximation, Eq. (34), for $n = 10$.

TABLE XI. Blackbody-radiation-induced depopulation rates (sec^{-1}) of states of sodium at 300 K. For values of n^* , see Table IV.

n	S	$P_{1/2}$	$P_{3/2}$	$D_{3/2}$	$D_{5/2}$
3	9×10^{-28}	4×10^{-12}	4×10^{-12}	484.9	479.7
4	7×10^{-3}	811.3	800.9	3954	3958
5	619.7	7689	7704	7743	7771
6	18420	27110	27200	16940	16990
7	64060	55490	55630	30870	30940
8	99540	74080	74240	41630	41700
9	112600	80950	81100	47180	47250
10	112100	80800	80930	49040	49090
11	105600	77100	77210	48600	48640
12	97010	71900	71990	46880	46920
13	88060	66250	66330	44530	44560
14	79580	60700	60770	41910	41940
15	71840	55480	55540	39190	39210
16	64890	50595 ^a	50595 ^a	36450 ^a	36450 ^a
17	58760	46226 ^a	46226 ^a	33940 ^a	33940 ^a
18	53360	42302 ^a	42302 ^a	31590 ^a	31590 ^a
19	48600	38791 ^a	38791 ^a	29420 ^a	29420 ^a
20	44400	35653 ^a	35653 ^a	27420 ^a	27420 ^a
25	29540	24252 ^a	24252 ^a	19710 ^a	19710 ^a
30	20950	17496 ^a	17496 ^a	14780 ^a	14780 ^a

^aFine structure neglected in calculation of depopulation rates for this state.

TABLE XII. Blackbody-radiation-induced depopulation rates (sec^{-1}) of states of potassium at 300 K. For values of n^* , see Table V.

n	S	$P_{1/2}$	$P_{3/2}$	$D_{3/2}$	$D_{5/2}$
3				0.33	0.31
4	9×10^{-20}	2×10^{-10}	3×10^{-10}	5 034	5 023
5	0.282	19.69	21.18	19 120	19 140
6	1 815	6 677	6 803	43 370	43 400
7	25 690	44 180	44 280	61 690	61 640
8	70 150	83 210	83 100	69 920	69 820
9	100 700	101 000	100 800	71 060	70 940
10	110 700	103 300	103 100	69 000	68 890
11	109 000	98 680	98 440	65 690	65 590
12	102 300	91 520	91 310	62 340	62 250
13	93 800	84 050	83 870	59 500	59 420
14	85 160	77 190	77 040	56 920	56 860
15	77 020	71 280	71 140	53 580	53 520
16	69 500	63 890 ^a	63 890 ^a	45 250 ^a	45 250 ^a
17	62 890	57 920 ^a	57 920 ^a	41 620 ^a	41 620 ^a
18	57 040	52 640 ^a	52 640 ^a	38 350 ^a	38 350 ^a
19	51 870	47 980 ^a	47 980 ^a	35 400 ^a	35 400 ^a
20	47 310	43 870 ^a	43 870 ^a	32 750 ^a	32 750 ^a
25	31 220	29 270 ^a	29 270 ^a	22 930 ^a	22 930 ^a
30	21 990	20 810 ^a	20 810 ^a	16 890 ^a	16 890 ^a

^aFine structure neglected in calculation of depopulation rate for this state.

programs, and to Thomas F. Gallagher for a copy of his Bates-Damgaard program.

APPENDIX A: DYNAMIC STARK SHIFT FROM TIME-DEPENDENT PERTURBATION THEORY

In this appendix, we outline the development of Eq. (2), the basic equation for the dynamic Stark shift, starting from the time-dependent Schrödinger

equation. In Sec. I, we treat the case of a near-resonant perturbation, using the rotating-wave approximation. Hence we deal in this section only with the resonant term of Eq. (2); the anti-resonant term in Eq. (2) is omitted. Because the resonant term has a pole on resonance, its validity is a matter of concern. Section I answers those concerns. We demonstrate that, when the resonant term in Eq. (2) is integrated over an interval

TABLE XIII. Blackbody-radiation-induced depopulation rates (sec^{-1}) of states of rubidium at 300 K. For values of n^* , see Table VI.

n	S	$P_{1/2}$	$P_{3/2}$	$D_{3/2}$	$D_{5/2}$
4				1.4×10^{-3}	1.0×10^{-3}
5	4×10^{-19}	2×10^{-7}	5×10^{-7}	2 746	2 790
6	0.3717	216.0	280.6	22 470	22 720
7	1 917	12 920	13 690	48 700	48 260
8	27 100	45 030	44 740	65 320	64 280
9	73 250	72 440	70 990	72 410	71 200
10	103 500	85 350	83 490	72 900	71 730
11	112 700	87 490	85 660	70 300	69 260
12	110 500	84 260	82 620	66 190	65 290
13	103 400	78 790	77 370	61 610	60 850
14	94 660	72 630	71 420	57 080	56 430
15	85 820	66 520	65 480	52 830	52 270
16	77 520	60 730	59 850	48 230	47 750
17	70 000	55 430	54 670	44 380	43 960
18	63 300	50 640	50 000	40 880	40 520
19	57 370	46 360	45 800	37 710	37 400
20	52 140	42 520	42 040	34 860	34 580
25	33 830	28 670	28 410	24 250	24 100
30	23 510	20 480	20 330	17 740	17 650

TABLE XIV. Blackbody-radiation-induced depopulation rates (sec⁻¹) of states of cesium at 300 K. For values of n^* , see Table VII.

n	S	$P_{1/2}$	$P_{3/2}$	$D_{3/2}$	$D_{5/2}$
5				1.778	0.8985
6	2×10^{-16}	1.410	2.420	2627	2931
7	1.34	3929	4402	1520	15070
8	2790	12300	10910	3782	36510
9	30790	27620	25580	57270	55110
10	76380	44580	43140	67280	65040
11	104500	55370	54450	69850	67810
12	112400	59920	59300	68420	66680
13	109600	60370	59920	65040	63570
14	102300	58510	58160	60960	59730
15	93560	55490	55200	56920	55910
16	84760	51990	51750	52670	51790
17	76590	48370	48160	48570	47820
18	69180	44830	44650	44780	44140
19	62580	41490	41330	41300	40760
20	56740	38390	38240	38150	37680
25	36350	26470	26360	26340	26100
30	24990	19090	19010	19090	18960

containing the resonance, it gives the same answer as the exact treatment. The Cauchy principal value of the integral is understood.

In Sec. II, we treat the case of a nonresonant perturbation. We obtain Eq. (2) as the result, including both the resonant and antiresonant terms.

1. The near-resonant perturbation

We follow the approach of Sargent *et al.*,⁴⁴ treating a two-level atom in the rotating-wave approximation. The two relevant levels, a and b , have a separation

$$\hbar\omega_0 = \hbar\omega_a - \hbar\omega_b = E_a - E_b > 0. \quad (\text{A1})$$

In the presence of the harmonic perturbation $V(t) = V_0 \cos\omega t$, the time-dependent Schrödinger equation for the amplitudes a and b is

$$i\dot{a} = (\omega_a - i\frac{1}{2}\gamma_a)a + \frac{1}{2}(e^{i\omega t} + e^{-i\omega t})V_b, \quad (\text{A2a})$$

$$i\dot{b} = (\omega_b - i\frac{1}{2}\gamma_b)b + \frac{1}{2}(e^{-i\omega t} + e^{i\omega t})V_a. \quad (\text{A2b})$$

The decay terms γ_a and γ_b treat spontaneous decay. We make the substitutions

$$C_a = ae^{i\omega_a t}, \quad (\text{A3a})$$

$$C_b = be^{i\omega_b t}, \quad (\text{A3b})$$

and seek a solution of the form

$$C_b(t) = e^{i\mu t}. \quad (\text{A4})$$

Since μ is complex, we have not made any assumptions about the magnitude of $C_b(t)$. The solutions of Eq. (A2) for $C_a(t)$ and μ , in the rotating wave approximation, are

$$C_a(t) = \left(\frac{-2\mu + i\gamma_b}{V} \right) e^{i(\mu - \omega + \omega_0)t}, \quad (\text{A5})$$

and

TABLE XV. Calculated blackbody-radiation-induced depopulation rates of states of sodium at 300 K. (Units are 10^3 sec^{-1} .)

State	Other work	This work	
		Exact calc.	High- n approx.
17P	44.1 ^a	46.2	70
18P	39.1 ^a	42.3	63
11S	97.8 ^b	105.6	21.8
21S	35.3 ^b	40.7	52.6
15 ($L=14$)	75.7 ^b	76.2	90.2
20 ($L=19$)	47.7 ^b	47.4	50.8

^aReference 1.

^bReference 3.

TABLE XVI. Blackbody-radiation-induced dynamic Stark shifts (Hz) in Rydberg states of helium. High-precision measurements of intervals among these states were reported in Ref. 29. Listed here is the sum of shifts caused by a 300 K apparatus and a 1400 K cathode, weighted by their respective solid angles.

n	1D	3D	$^1,^3F$	$^1,^3G$
6	465	-318	365	470
7	580	138	944	1143
8	1492	706	1488	1712
9	1897	1208	1908	2115
10	2210	1632	2226	2406
11	2453	1975	2469	2620

$$\mu_{1,2} = \frac{1}{2}(\omega - \omega_0 + i\gamma_{ab}) \pm \frac{1}{2}[(\omega - \omega_0 + i\delta_{ab})^2 + V^2]^{1/2}. \quad (\text{A6})$$

Here γ_{ab} and δ_{ab} are defined by

$$\gamma_{ab} = \frac{1}{2}(\gamma_a + \gamma_b), \quad (\text{A7})$$

$$\delta_{ab} = \frac{1}{2}(\gamma_a - \gamma_b). \quad (\text{A8})$$

The general solution is a linear combination of the two solutions in Eq. (A6). The appropriate linear combination is determined by the initial conditions. We choose

$$C_a(0) = 1, \quad C_b(0) = 0. \quad (\text{A9})$$

These initial conditions mean that the initial wave function is entirely state a ; hence, a is the *per-*turbed state and b is the *per-*turbating state. One then obtains

$$|\mu_2/\mu_1| = \left| \left\{ \omega - \omega_0 - [(\omega - \omega_0)^2 + V^2]^{1/2} \right\} \left\{ \omega - \omega_0 + [(\omega - \omega_0)^2 + V^2]^{1/2} \right\}^{-1} \right|. \quad (\text{A13})$$

For $\omega = \omega_0$ the ratio is unity. For $\omega - \omega_0 < -V$, the ratio is much greater than one, while for $\omega - \omega_0 > V$ the ratio is much less than one. Hence, when ω is below (above) resonance, the second (first) term in Eq. (A12) is dominant. Dropping the smaller term, we obtain for $\omega - \omega_0 < -V$,

$$a(t) \simeq -(\mu_2/\mu) e^{-i(\omega_a + \mu_2)t} \quad (\text{A14a})$$

and for $\omega - \omega_0 > V$,

$$a(t) \simeq (\mu_1/\mu) e^{-i(\omega_a + \mu_1)t}. \quad (\text{A14b})$$

Instead of an energy ω_a , Eq. (14) reveals an "effective energy" $\omega_a + \delta\omega_a$, where the dynamic Stark shift $\delta\omega_a$ is μ_1 (μ_2) for ω below (above) resonance. Both frequency components of Eq. (A12) are always present, but, except near resonance, the magnitudes of the two components are grossly unequal. As we tune through resonance, the relative magnitudes of the two components reverse. The "shift" executes a finite jump of magnitude V at $\omega = \omega_0$ from one branch to the other. For $|V/(\omega - \omega_0)| \ll 1$ we can expand μ_1 and μ_2 to obtain

$$\delta\omega_a = -\frac{1}{2}V^2/(\omega - \omega_0). \quad (\text{A15})$$

This expression differs from Eq. (2) in the omission of the antiresonant term. This is a consequence of the rotating-wave approximation.

We now consider the total shift caused by a perturbation having a distribution of frequencies in a symmetrical frequency interval centered on resonance ($\omega = \omega_0$). We calculate the total shift by integrating over the interval $-\Delta_0 \leq \omega - \omega_0 \leq \Delta_0$. There are two ways to calculate the total shift. We can integrate the exact expressions for the

$$C_b(t) = \frac{1}{2}V\mu^{-1}(e^{i\mu_2 t} - e^{i\mu_1 t}), \quad (\text{A10a})$$

$$C_a(t) = \mu^{-1}e^{-i(\omega - \omega_0)t} \times [(-\frac{1}{2}i\gamma_b + \mu_1)e^{i\mu_1 t} - (-\frac{1}{2}i\gamma_b + \mu_2)e^{i\mu_2 t}], \quad (\text{A10b})$$

where μ is defined as

$$\mu \equiv \mu_1 - \mu_2 = [(\omega - \omega_0 + i\delta_{ab})^2 + V^2]^{1/2}. \quad (\text{A11})$$

At this point, we neglect damping. We now let $\gamma_a, \gamma_b \rightarrow 0$ and use Eq. (A3b) to obtain for the Schrödinger amplitude a

$$a(t) = (\mu_1/\mu)e^{-i(\omega_a + \mu_2)t} - (\mu_2/\mu)e^{-i(\omega_a + \mu_1)t}. \quad (\text{A12})$$

The two frequency components of Eq. (A12) have relative amplitudes whose ratio is

shift $\mu_{1,2}$ over the frequency interval, or we can use the approximation (A15), which is just the resonant term of Eq. (2) of the main text. In the rest of this section, we demonstrate that these two approaches yield identical results. Hence the resonant term of Eq. (2) does not cause any trouble when integrated over a frequency interval containing the resonance.

We want to calculate

$$\delta\omega_a = \int_{\omega_0 - \Delta_0}^{\omega_0} \lambda_1 d\omega + \int_{\omega_0}^{\omega_0 + \Delta_0} \lambda_2 d\omega. \quad (\text{A16})$$

Let us assume that the perturbation V^2 varies slowly with frequency in the region of the resonance, and we can use a truncated Taylor series expansion

$$V^2 = c_0 + c_1(\omega - \omega_0) + \dots \quad (\text{A17})$$

Using the definitions (A6) for μ_1 and μ_2 , we obtain

$$\begin{aligned} \delta\omega_a = & \int_{-\Delta_0}^0 \frac{1}{2}(\omega - \omega_0)d(\omega - \omega_0) + \int_0^{\Delta_0} \frac{1}{2}(\omega - \omega_0)d(\omega - \omega_0) \\ & + \frac{1}{2} \int_{-\Delta_0}^0 [(\omega - \omega_0)^2 + V^2]^{1/2} d(\omega - \omega_0) \\ & - \frac{1}{2} \int_0^{\Delta_0} [(\omega - \omega_0)^2 + V^2]^{1/2} d(\omega - \omega_0). \end{aligned} \quad (\text{A18})$$

The first two terms cancel. We evaluate the last two terms to lowest order in c_1 . Substituting Eq. (A17) in Eq. (A18), we expand to obtain

$$\begin{aligned} & [(\omega - \omega_0)^2 + c_0 + c_1(\omega - \omega_0)]^{1/2} \\ & \simeq [(\omega - \omega_0)^2 + c_0]^{1/2} + \frac{1}{2}c_1(\omega - \omega_0)(\Delta^2 + c_0^2)^{1/2}. \end{aligned} \quad (\text{A19})$$

Equation (A18) then becomes

$$\begin{aligned} \delta\omega_a = & \frac{1}{2} \int_{-\Delta_0}^0 (\Delta^2 + c_0)^{1/2} d\Delta - \frac{1}{2} \int_0^{\Delta_0} (\Delta^2 + c_0)^{1/2} d\Delta \\ & + \frac{1}{4} c_1 \int_{-\Delta_0}^0 (\Delta^2 + c_0)^{-1/2} \Delta d\Delta \\ & - \frac{1}{4} c_1 \int_0^{\Delta_0} (\Delta^2 + c_0)^{-1/2} \Delta d\Delta, \end{aligned} \quad (\text{A20})$$

where $\Delta = \omega - \omega_0$.

The first two terms cancel, while the last two terms yield

$$\delta\omega_a = \frac{1}{2} c_1 [c_0 - (\Delta_0^2 + c_0)^{1/2}]. \quad (\text{A21})$$

If the spectrum of the radiation is flat ($c_1 = 0$) and symmetrically distributed around the resonance, Eq. (21) demonstrates that the shift vanishes. If the interval over which we integrate is several times the resonance width, we have $\Delta_0^2 \gg c_0$ and the shift becomes

$$\delta\omega_a \cong -\frac{1}{2} c_1 \Delta_0. \quad (\text{A22})$$

If, instead of the exact (in the rotating-wave approximation) expression for the shift, $\mu_{1,2}$, one uses the approximate expression (A15), the total shift due to the perturbation is

$$\delta\omega_a = -\int_{-\Delta_0}^{\Delta_0} \frac{1}{4} (\omega - \omega_0)^{-1} [c_0 + c_1 (\omega - \omega_0)] d(\omega - \omega_0) \quad (\text{A23})$$

$$= -\frac{1}{4} c_0 \int_{-\Delta_0}^{\Delta_0} \frac{d\Delta}{\Delta} - \frac{1}{4} \int_{-\Delta_0}^{\Delta_0} c_1 d(\omega - \omega_0). \quad (\text{A24})$$

The first term, evaluated in the Cauchy principal value sense, yields zero, while the second term yields

$$\delta\omega_a = -\frac{1}{2} c_1 \Delta_0. \quad (\text{A25})$$

Note that Eq. (A25) is identical to Eq. (A22). We conclude that, although Eq. (A15) is, strictly speaking, only valid off resonance, it yields the correct result in the rotating-wave approximation

$$\int_{y-0.1}^{y+0.1} x^3 (e^x - 1)^{-1} (y - x)^{-1} dx = \lim_{\epsilon \rightarrow 0} \left(\int_{y-0.1}^{y-\epsilon} x^3 (e^x - 1)^{-1} (y - x)^{-1} dx + \int_{y+\epsilon}^{y+0.1} x^3 (e^x - 1)^{-1} (y - x)^{-1} dx + \text{corr}(y, \epsilon) \right). \quad (\text{B1})$$

The first and second terms on the right of Eq. (B1) were each evaluated as a sum of contributions in which the singularity was approached logarithmically; i.e., the intervals contributing to the first term were $[y - 0.1, y - 0.01]$, $[y - 0.01, y - 0.001]$, ..., $[y - 10\epsilon, y - \epsilon]$.

$\text{Corr}(y, \epsilon)$ represents a correction term which gives the contribution from the region $[y - \epsilon, y + \epsilon]$ to lowest order in ϵ . $\text{Corr}(y, \epsilon)$ is defined by

when integrated over the resonance region, using the Cauchy principal value.

2. The nonresonant perturbation

Wing and MacAdam⁴⁵ have treated the case of a multilevel atom subjected to a weak monochromatic nonresonant perturbation at frequency ω . They found an rf power shift in the transition $\omega_0 = \omega_a - \omega_b$:

$$\begin{aligned} \delta\omega_0 = & \frac{1}{4} \left[\sum_n |V_{an}|^2 \left(\frac{1}{\omega_a - \omega_n - \omega} + \frac{1}{\omega_a - \omega_n + \omega} \right) \right. \\ & \left. - |V_{bn}|^2 \left(\frac{1}{\omega_b - \omega_n - \omega} + \frac{1}{\omega_b - \omega_n + \omega} \right) \right]. \end{aligned} \quad (\text{A26})$$

We can identify the terms involving state k as a shift in the energy of state k ($k = a, b$), thereby obtaining Eq. (2) of the main text. We note in passing that in the field of Raman spectroscopy similar expressions occur for the dynamic polarizability tensor.

APPENDIX B: EVALUATION OF $F(y)$

The integral in Eq. (9) was evaluated as a sum of many integrals over segments of the range $0 \leq x \leq 30$. Each segment integral was calculated using a 32-point Gaussian quadrature subroutine.⁴⁶ The evaluation of the contribution from the relatively slowly varying regions $[0, y - 0.1]$ and $[y + 0.1, 30]$ was a straightforward task. However, a difficulty arises from the singularity at $x = y$. The contribution from the interval $[y - 0.1, y + 0.1]$ was evaluated in the following manner. The nonresonant term $(y + x)^{-1}$ was separated out and its contribution evaluated. The contribution of the resonant term $(y - x)^{-1}$ was evaluated using the Cauchy principal value. This approach is physically reasonable because the energy levels have a nonzero width when relaxation processes are taken into account. We obtain

$$\text{corr}(y, \epsilon) = \int_{y-\epsilon}^{y+\epsilon} x^3 (e^x - 1)^{-1} (y - x)^{-1} dx. \quad (\text{B2})$$

The factor $(y - x)^{-1}$ in the integrand varies rapidly and changes sign at the singularity. In contrast, the factor $x^3 (e^x - 1)^{-1}$ is well behaved. Expanding this latter factor in a Taylor series around $x = y$ and retaining the first two terms, we obtain

$$x^3(e^x - 1)^{-1} \approx y^3(e^y - 1)^{-1} + (x - y)\{y^2(e^y - 1)^{-1}[3 - ye^y(e^y - 1)^{-1}]\}. \quad (\text{B3})$$

This expression is inserted into Eq. (B2). The result is

$$\text{corr}(y, \epsilon) = y^3(e^y - 1)^{-1} \int_{y-\epsilon}^{y+\epsilon} (y-x)^{-1} dx - y^2(e^y - 1)^{-1}[3 - ye^y(e^y - 1)^{-1}] \int_{y-\epsilon}^{y+\epsilon} dx. \quad (\text{B4})$$

The first term in Eq. (B4) is zero by symmetry. The second term yields

$$\text{corr}(y, \epsilon) = -2\epsilon y^2(e^y - 1)^{-1}[3 - ye^y(e^y - 1)^{-1}]. \quad (\text{B5})$$

When all the contributions to $F(y)$ were added up, the result was quite insensitive to the value of ϵ . $F(y)$ varied by about one part in 10^7 when ϵ varied by three orders of magnitude ($10^{-5} \leq \epsilon \leq 10^{-2}$).

The integral $F(y)$ was evaluated with resolution $\Delta y = 0.1$ in the region $[0, 10]$, with $\Delta y = 1$ in the region $[10, 100]$, and with $\Delta y = 10$ in the region $[100, 1000]$. The resulting array was stored in a computer disk file for future use. The running time for the Fortran program on our Nova-2 mini-computer, which utilizes a software floating-point package, was several hours. To obtain the value of $F(y)$ in a subsequent program, we interpolated in the array of points by fitting a parabola to the local curve. For asymptotic values of y ($|y| < 0.1$ or $|y| > 1000$), we did not interpolate but instead used the relevant asymptotic closed-form expressions Eqs. (11) and (12). The approximation, Eq. (12), is extremely good for large y . For small y , the error introduced by Eq. (11) increases with y , rising to 1% at the $y = 0.1$ endpoint. Since $F(y)$ is small in this regime, this level of precision is satisfactory; moreover, it is probably comparable to the errors introduced by the interpolation procedure. A final source of error is the cutoff of the integration at the upper limit $x = 30$. It can be shown analytically that the error thus introduced is approximately one part in 10^7 .

¹T. F. Gallagher and W. E. Cooke, Phys. Rev. Lett. **42**, 835 (1979). See Sec. V A 1 of the text.

²F. Gounand, J. Phys. (Paris) **40**, 457 (1979).

³W. E. Cooke and T. F. Gallagher, Phys. Rev. A **21**, 588 (1980).

⁴E. J. Beiting, G. F. Hildebrandt, F. G. Kellert, G. W. Foltz, K. A. Smith, F. B. Dunning, and R. F. Stebbings, J. Chem. Phys. **70**, 3551 (1979).

⁵T. F. Gallagher and W. E. Cooke, Appl. Phys. Lett. **34**, 6 (1979).

⁶M. Gross, P. Goy, C. Fabre, S. Haroche, and J. M. Raimond, Phys. Rev. Lett. **43**, 343 (1979).

⁷P. R. Koch, H. Hieronymus, A. F. J. Van Raan, and W. Raith, Phys. Lett. **75A**, 273 (1980).

⁸W. Spencer and D. Kleppner (private communication).

⁹H. Figger, G. Leuchs, R. Straubinger, and H. Walther, Opt. Commun. **33**, 37 (1980).

¹⁰M. Arditi and T. R. Carver, Phys. Rev. **124**, 800 (1961).

¹¹J. Dupont-Roc, N. Polonsky, C. Cohen-Tannoudji, and A. Kastler, C. R. Acad. Sci. Ser. B **264**, 1811 (1967).

¹²A. Kastler, J. Opt. Soc. Am. **53**, 902 (1963).

¹³J. P. Barrat and C. Cohen-Tannoudji, J. Phys. (Paris) **22**, 329 (1961); **22**, 443 (1961).

¹⁴B. S. Mathur, H. Tang, and W. Happer, Phys. Rev. **171**, 11 (1968); W. Happer and B. S. Mathur, *ibid.* **163**, 12 (1967).

¹⁵W. Heitler, *The Quantum Theory of Radiation* (Oxford, London, 1954).

¹⁶V. Weisskopf and E. Wigner, Z. Phys. **63**, 54 (1930).

¹⁷C. H. Townes and A. L. Schawlow, *Microwave Spectroscopy* (Dover, New York, 1975), pp. 273-283. In Eqs. (10)-(77), W_2 should read W_n .

¹⁸S. H. Autler and C. H. Townes, Phys. Rev. **100**, 703

(1955).

¹⁹F. Bloch and A. Siegert, Phys. Rev. **57**, 522 (1940); for a treatment to much higher order, see J. Shirley, Phys. Rev. **138B**, 979 (1965).

²⁰E. T. Jaynes and F. W. Cummings, Proc. IRE **51**, 89 (1963).

²¹I. S. Gradshteyn and I. M. Ryzhik, *Table of Integrals, Series and Products* (Academic, New York, 1965), p. 325, Eq. (2).

²²H. Bethe and E. Salpeter, *Quantum Mechanics of One- and Two-Electron Atoms* (Springer, Berlin, 1957).

²³D. R. Bates and A. Damgaard, Philos. Trans. R. Soc. London **242**, 101 (1949).

²⁴W. E. Lamb, Jr. and T. M. Sanders, Jr., Phys. Rev. **119**, 1901 (1960).

²⁵J. E. Bayfield, Phys. Rep. **51**, 317 (1979).

²⁶M. L. Zimmerman, M. G. Littman, M. M. Kash, and D. Kleppner, Phys. Rev. A **20**, 2251 (1980).

²⁷S. Bashkin and J. O. Stoner, Jr., *Atomic Energy Level and Grotrian Diagrams* (North-Holland, Amsterdam, 1976), Vols. I and II.

²⁸C. E. Moore, *Atomic Energy Levels* (National Bureau of Standards, Washington, D. C., 1971).

²⁹J. W. Farley, K. B. MacAdam, and W. H. Wing, Phys. Rev. A **20**, 1754 (1979).

³⁰*Handbook of Chemistry and Physics*, 54th ed. (CRC Press, Cleveland, 1973), p. A-114, Eq. (38).

³¹W. L. Wiese, in *Progress in Atomic Spectroscopy, Part B*, edited by W. Hanle and H. Kleinpoppen (Plenum, New York, 1979), pp. 1101-1155.

³²A. Burgess and M. J. Seaton, Rev. Mod. Phys. **30**, 992 (1958).

³³A. Burgess and M. J. Seaton, Mon. Not. R. Astron. Soc. **120**, 121 (1960).

- ³⁴G. Peach, Mem. R. Astron. Soc. 71, 13 (1967).
- ³⁵U. Fano and J. W. Cooper, Rev. Mod. Phys. 40, 441 (1968).
- ³⁶J. W. Farley, A. H. Johnson, and W. H. Wing, J. Phys. E 13, 848 (1980).
- ³⁷S. A. Lee, J. Helmcke, J. L. Hall, and B. P. Stoicheff, Opt. Lett. 3, 141 (1978).
- ³⁸M. Rosenbluh, R. Panock, B. Lax, and T. A. Miller, Phys. Rev. A 18, 1103 (1978).
- ³⁹S. L. Kaufman, W. E. Lamb, Jr., K. R. Lea, and M. Leventhal, Phys. Rev. A 4, 2128 (1971).
- ⁴⁰S. Klarsfeld, Phys. Lett. 30A, 382 (1969).
- ⁴¹R. S. Van Dyck, Jr., P. B. Schwinberg, and H. G. Dehmelt, Phys. Rev. Lett. 38, 310 (1977).
- ⁴²Lifetimes taken from A. Lindgard and S. E. Nielsen, At. Data Nucl. Data Tables 19, 533 (1977).
- ⁴³P. L. Richards, Phys. Scr. 21, 610 (1980); D. T. Wilkinson, *ibid.* 21, 606 (1980).
- ⁴⁴M. Sargent, M. O. Scully, and W. E. Lamb, Jr., *Laser Physics* (Addison-Wesley, Reading, Massachusetts, 1977).
- ⁴⁵W. H. Wing and Keith B. MacAdam, in *Progress in Atomic Spectroscopy, Part A*, edited by W. Hanle and H. Kleinpoppen (Plenum, New York, 1978), pp. 491–527.
- ⁴⁶Subroutine DQG32 in *IBM Scientific Subroutine Package*, 5th ed. (1970), pp. 299–303; IBM Corporation, Technical Publications Department, 112 East Post Road, White Plains, New York 10601. For reference, see V. J. Krylov, *Approximate Calculation of Integrals* (MacMillan, New York/London, 1962), pp. 100–111 and 337–340.